UNIVERSITY *of the*
WESTERN CAPE

The application of geophysics and petrophysics to perform a reservoir characterisation on selected wells in the Orange Basin

By:

Uzair Adam

Submitted in partial fulfilment of the requirements for the degree of MAGISTER SCIENTAE (MSc) in the Department of Earth Sciences, University of the Western Cape, Cape Town, South Africa

Supervisor: Professor Mimonitu Opuwari

19 September 2022

Council for Geoscience

Abstract

Three wells located in the Orange Basin on the west coast of South Africa were modelled and characterised using petrophysical and geophysical data. This study is focussed on providing a solution to performing a reservoir characterisation using modern software and techniques in an area where data were collected three decades ago. Using the 2-D seismic data from the seismic survey, a triangulated study area was created. Utilising the acquired 2-D seismic data, re-analysing and up scaling the well logs to create a static model to display the petrophysical properties essential for reservoir characterisation. This was carried out using Interactive Petrophysics and Petrel software packages. A total of two target areas were identified across all three wells, except A-C2, which only had one target area. The two areas of interest were identified between the M2KI and 13At1, and the TFLUVIAL and Bottom of Log in A-C3. Target Area 1 was present in all three wells and at a shallower depth than Target Area 2. In Target Area 1, three facies were identified, namely: sand, silt and shale. Target Area 1 consisted mostly of silty shale and shaly silt. Although, there was a thin sand package at the top of the target area Target Area 2, had the same facies as Target Area 1, except with an additional facies, a basement facies, which made up the predominant space in Target Area 2. Target Area 2 had considerably thicker sand layers and thus the porosity and permeability were slightly better, but overall still poor. The porosity in Target Area 1 ranged from 0,0001 to 0,45 m^3/m^3. Whereas, the porosity in Target Area 2 ranged from 0,0002 to 0,23 m^3/m^3. This compared to the permeability in Target Area 1, which ranged from 0,001 to 571,25 mD. Whereas, the permeability in Target Area 2, ranged from 0 to 20,1 mD. The overall poor permeability and porosity in the triangulated area is a result of a high concentration of clay in the matrix in some of the sand layers. In terms of economic potential and Target Area 2 would be the area to look at, as the water saturation is lower and the porosity and permeability are slightly better. The recoverable gas in Target Area 1 is 95 057 cubic metres. Although the recoverable gas in Target Area 2 is slightly better, with a volume of 151 923 cubic metres, overall it is still low. This study has shown for the first time through the integration of petrophysical and geophysical datasets that the southern part of the Orange Basin is not economically viable.

Declaration

I declare that ***The application of geophysics and petrophysics to perform a reservoir characterisation on a selected area and selected wells in the Orange Basin*** is my own work, that it has not been submitted before any degree or examination in any other university, and that all the sources I have used or quoted have been indicated and acknowledged as complete references.

Uzair Adam

19 September 2022

Keywords

Orange Basin
Hydrocarbon
Seismic Interpretation
Wireline logs
Petrophysics
Modelling
Reservoir Characterisation
Facies
Volume of shale
Porosity
Permeability
Storage capacity

Acknowledgments

Before I started my dissertation research on the Orange Basin, I had a great interest and desire to get involved in marine research and learn the techniques of petroleum geology and marine geophysics. I am grateful to the Council for Geoscience for funding my project and the resources they allowed me to use. Thank you to the Petroleum Agency of South Africa for all the assistance and allowing me to work on the data collected.

I would like to express my gratitude to my supervisor, Professor Minomitu Opuwari for his continuous support, advice and guidance through the project. Although he was a hands-off supervisor, he provided me with the necessary help and patience when needed. I cannot thank Blessing Afolayan enough for his patience, long hours and support in this project. His assistance in this project has taught me so much, particularly interpreting seismic data and gaining knowledge in Petrel and Interactive Petrophysics.

Thank you to my colleagues at the Council for Geoscience for their support and granting me time off during quiet work periods. In particular I'd like to thank Michael Machutchon for his continuous mentorship and guidance in both my project and my career.

A loving thanks to my friends for their continuous words of encouragement and motivation, especially in the stressful times.
I am indebted to my family for the continuous love, motivation and help in my academic career.

Table of Contents

List of figures

List of tables

1. CHAPTER 1: Introduction

Reservoir characterisation has matured over three generations. Initially, it was based solely on petrophysics, then to geologic analogues, and more recently to multidisciplinary integration (Ma, 2011). In recent years, integrated approaches have been proven time and time again to be efficient in scientific studies, especially in generating petroleum reservoir characterisation models. The multidisciplinary approach links all available geologic engineering and geophysical data to produce a better reservoir model (Evans, 1996). This approach makes use of the complementary strengths of two independent measures and combines them to create an important synergy. One of these strengths is using seismic data to provide information about the variations between wells, which is not available when only using well log data.

Reservoir characterisation is a technique to predict the behaviour of a reservoir, by quantifying and mapping the reservoir properties in the wells of the basin. This is carried out by integrating, analysing, and understanding all the data that is available (Civan, 2007). Linking the interpretation of different geophysical properties with the evaluation of petrophysical properties creates a detailed approach to reservoir characterisation (Bashir *et al*., 2021). This can then indicate the reservoir fluid behaviour and be used to find the optimal production techniques that are able to maximise production.

Seismic data has been extensively used to help in the exploration of hydrocarbons by providing in-fill data on the rock properties between wells. There are multiple inversion techniques that use seismic data for property prediction based on the correlation between the property and the seismic (impedance, porosity, and acoustic) (Africa, 2016). Seismic data is inverted to create an image of the desired character through the media. Traditionally, seismic inversion has been performed with the use of well logs, which has issues in its derivation steps (e.g. wavelet extraction and its propagation through media) (Shahbazi *et al*., 2019).

In recent times, reservoirs are becoming more complex, and need to explore deeper or revisit old/previously studied reservoirs is occurring more frequently. Currently,

because in many areas it is perceived that “easy oil” is being produced, the challenges now involve complex geology, or the locations are more difficult. These challenges would lead to a need to improve the standard for data analysis. Considerate research has been undertaken in the last two decades in the Orange Basin by (Mabona, 2012, Africa, 2016, Williams, 2018), which focussed on reservoir characterisations of various wells located in the northern region of the Orange Basin. Paton *et al*. (2007) focused on the controls of hydrocarbon generation and leakage in the southern region of the Orange Basin.

A successful discovery of hydrocarbons in Namibia made by Shell earlier in 2022 (Bate, 2022), raises the question of whether that play continues further south into the Orange Basin. If it does, revisiting previously acquired data could lead to a better understanding of the Orange Basin in greater detail and the extent of the plays in this basin. Multiple data types are used in this study, and the correlation between seismic interpretation and wireline logs, forms an informative basis in the characterisation of the reservoirs in the selected wells of this study.

These three wells along with the seismic survey lines create a triangulated area, with an area of approximately 86.4 km^2. By performing petrophysical analyses on the three wells, the reservoir properties can be calculated. Seismic interpretation will be used to map the reservoir properties over the study area between the well bores. This will lead to the building of the static models of the study area using the interpreted petrophysical and geophysical data. The final goal is to determine if there is an economic potential for future exploration in the study area.

1.1 Location of study area

The Orange Basin is situated on the western offshore of South Africa and has an approximated area of 160 000 km^2 (PASA, 2019). It is the largest (in area and volume) offshore basin of the South African offshore basins, extending about 500 km on the west coast and is largely underexplored with an average of one well per 4000 km^2 (PASA, 2019), even though several petroleum systems are known to be operating.

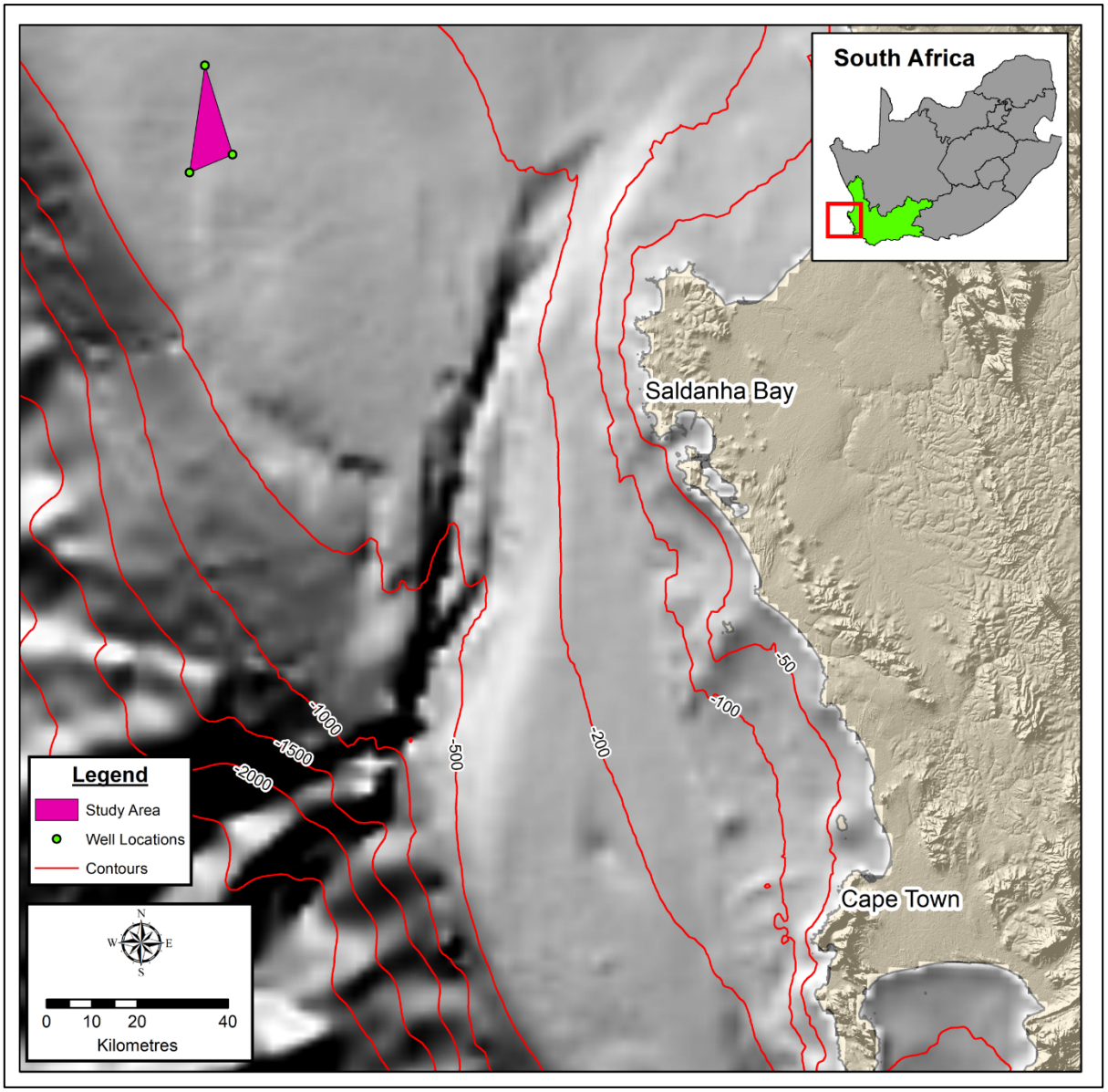

Figure 1.1. Locality map of the study area, bathymetry adapted from De Wet (2012). Contours are in metres.

The three wells used in this study are A-C1, A-C2 and A-C3. Wells A-C1 and A-C2 are in Block 3A/4A, whereas A-C3 is in Central Orange Basin. These wells are in the southern part of the Orange Basin on the West Coast of South Africa and have not been extensively explored. These three wells create a triangulated area, with an area of approximately 86.4 km^2. Table 1.1 below summarises the geographical co-ordinate and wireline depths of the corresponding wells.

Table 1.1 Geographical co-ordinates of the wells and wireline depths.

Well names	Block	Locations	Depths (m)
A-C1	Block 4	Latitude: 32º 30’ 29,53” S Longitude: 16º 53’ 29,97” E	4139
A-C2	Block 4	Latitude: 32º 19’ 55,38” S Longitude: 16º 49’ 25,25” E	3613
A-C3	Central Orange Basin	Latitude: 32º 32’ 43,04” S Longitude: 16º 47’ 30,24” E	4150.2

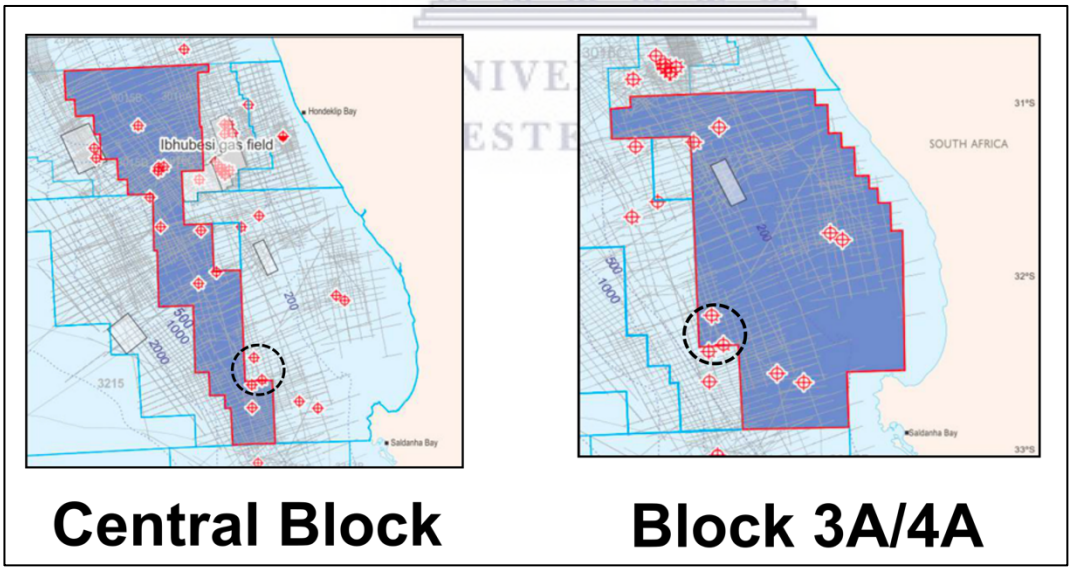

Figure 1.2. Image showing the two blocks where the wells are located.

1.2 Problem statement

The Orange Basin is the largest basin in Southern Africa covering an area of approximately 160 000 km^2. The basin is considered underexplored with one well every 4000 km^2 and these wells were drilled in the 1970s – 1990s (Broad *et al*., 2006). However, a recent gas discovery in Namibia made by Shell, in addition to the existing Kudu and Ibhubesi gas fields, poses the question of: Were the identification hydrocarbon reservoirs missed due to the limited technology at the time of exploration and is there a economic potential in three wells that were previously classified as dry? Revisiting previously investigated wells is important, as it provides an opportunity to potentially identify new areas and/or change existing areas, that previous studies may have missed (Ma, 2011).

1.3 Aim of the study

The aim of this study is to use modern software and techniques to perform a reservoir characterisation on previously collected data. This would be an independent study that would be carried out by the correlation of the interpretation of petrophysical data with the interpretation of seismic data in the three wells selected (A-C1, A-C2 and A-C3) and use these characteristics to generate static reservoir models of the target areas identified in the three wells and the triangulated area.

1.3.1 Objectives

The objective of this study is to determine whether there is an economic potential in the study area, by performing petrophysical analyses on the three wells which are all intersecting a seismic survey. Building static models of the study area using the petrophysical and geophysical data will be the key objective to determining this economic potential.

To achieve this, the data sets must be quality checked, ensuring the data sets are complete, and information not required is removed. The geophysical analysis includes performing a detailed seismic interpretation on the 2-D seismic dataset, identifying horizons and faults. The petrophysical analysis includes carrying out a petrophysical

evaluation using the conditioned logs to determine reservoir zones and attributes. The last objective would be linking the interpretation of the seismic data with the log calculations from the well log data, to produce static reservoir models. These models would be discussed, and the economic potential will be determined.

2. CHAPTER 2: Literature review

The exploration of the Orange Basin began in 1974 with the Kudu Gas Field discovery in the southern offshore Namibia (PASA, 2019). During the 1980s, the regional seismic and geologic data collected at the time were interpreted and published (Austin and Uchupi, 1982, Gerrard and Smith, 1982). This was before the application of modern seismic and sequence stratigraphy data or using these methods together. The geological and morphological characteristics of the South Atlantic Margin were studied by Brown *et al*. (1995). Included in their study was the first-time use of sequence stratigraphy in conjunction with the conventional exploration techniques at the time. They found that creating a regional sequence framework could greatly aid in the understanding of the depositional effects related to the cyclic changes in sea level under different tectonic and sediment supply conditions. Hence, sequence stratigraphy is important when exploring for stratigraphic or combination traps.

There have been various studies carried out in the Orange Basin over the last two decades, but the area is still largely underexplored, with one well located every 4000 km^2 (Broad *et al*., 2006). However, only in the last decade did studies become multi-disciplinary. Multi-disciplinary studies have been found to be the most effective and efficient method of answering geological problems and contributing detailed information to the field of study. In the oil and gas field, these multi-disciplinary studies are particularly important and are being implemented because they provide a more detailed analysis and thus greatly reduce the risk associated with the uncertainty of drilling.

The Orange Basin is a good frontier for hydrocarbon exploration for several reasons. Firstly, there is extensive data available, including 2D and 3D seismic lines in the ultra-deep marine region. Secondly, more than 15 wells have been drilled and majority of the wells are located on the shelf. Thirdly, proven gas plays (Kudu and Ibhubesi gas fields) provide concrete evidence that there is a high potential for petroleum, particularly natural gas, in the basin. Different hydrocarbon exploration techniques have been applied to the hydrocarbon potential in reservoir rocks in the Orange Basin. These techniques included, sedimentology, geochemistry, geophysical, petrophysical and

structural (Muntingh and Brown, 1993, Jungslager, 1999, Campher, 2009, Opuwari, 2010, Mabona, 2012, Africa, 2016, Williams, 2018, Yelwa et al., 2022) have contributed to the understanding of this basin. Majority of these studies were focused on wells located near the Kudu and Ibhubesi (Mabona, 2012, Williams, 2018).

A multi-disciplinary study was undertaken by Opuwari (2010) in the Orange Basin. He integrated and compared results from core analysis, production data and petrography studies, for the evaluation of petrophysical parameters from wireline logs. Opuwari (2010), combined these techniques and used ten wells to build an effective reservoir model. Opuwari (2010), identified 28 sandstone reservoirs, with 24 four of them being gas bearing and four wet within the Albian age depth interval of 2800 m to 3500 m. Opuwari (2010), used the core data to identify six lithofacies and determine the porosity and permeability within these wells. The average porosity and permeability were determined to be 10 – 22 % and 60 mD, respectively. The average water saturation ranged between 23 – 69 % (Opuwari, 2010).

Four wells located in the Shungu Shungu gas field in the Orange Basin were found to be dry wells as well (Mabona, 2012). However, Mabona (2012) used an integrated study focused on the analysis of cores, wireline logs and seismic to produce a suitable reservoir model. In addition, Mabona (2012) made use of petrophysics software and seismic to better understand why the area had dry wells. Similarly to how Mabona (2012) incorporated a multi-disciplinary study to not only characterise these wells, but why they were dry is exactly what will be carried out in this study. Using modern technology and various petroleum models could greatly aid in reaching a different conclusion about reservoir characterisation.

Mugivhi (2017) conducted a study on five wells located in block 2A and 2B in Mid-Orange Basin. The aim was to contribute to the understanding of the Lower Cretaceous reservoir, whilst providing insights about its economic potential. The techniques included the analysis of core data and well log data. Despite the data being different to this current project, Mugivhi (2017) still proved that an integrated study is efficient. Mugivhi (2017) concluded that the hydrocarbon volume varied from 67.89 m^3 to 176.00 m^3 and that good to very good reservoir qualities were found in some of the

zones of three wells (A-J1, A-K1 and A-H1). However, wells A-D1 and K-A2 displayed poor reservoir qualities.

Williams (2018) performed a reservoir characterisation on well A-F1, located in the northern part of the basin in block 1. The aim was to determine if the aeolian play for the Kudu gas field extends southwards into the South African portion of the Orange River Basin and if it is economically probable. The data used in this project is very similar to what Williams (2018) used. The only difference is that Williams (2018) used 3D seismic data compared to this study, which is using 2D seismic data, because 2D seismic data was not available in this area. It was found that although there were minor amounts of hydrocarbon shows in the reservoir, there was also a high water saturation in the sandstones and thus the reservoir was deemed uneconomical.

A recent study carried out by Yelwa *et al*. (2022) analysed and interpreted shale sediments from four explorations well locations in the Orange Basin. The shale sediments were analysed, using geochemistry, to determine organic matter characteristics and their suitability as gas resources. Yelwa *et al*. (2022) identified that the sediments consisted of primarily Type III kerogen, organic matter than primarily produces both wet and dry gas when they mature. These findings are promising for shale gas exploration, as hydrocarbon (particularly gas) exploration is developing in the Orange Basin.

This project is particularly interesting, because it is the first comprehensive study conducted on wells A-C1, A-C2 and A-C3 since the early 1990s, when SOEKER initially drilled them. Furthermore, seismic lines will be used with the intention of identifying target areas, which will be mapped across an area of approximately 86.4 km^2 . Referring back to Brown *et al*. (1995), the use of sequence stratigraphy with seismic data greatly improves the understanding and quality of the characterisation of a reservoir, particularly when stratigraphic traps are involved. The tracking of the reservoir will be carried out by linking the sequence stratigraphy not only in the seismic lines but also with the well logs. Thus, determining if the three wells are connected to the same reservoir(s) or not.

3. CHAPTER 3: Geological background of the Orange Basin

3.1 Tectonic evolution of the basin

The Orange Basin is part of the western margin, which is a passive continental margin of southern Africa. This passive margin was formed during the breakup of Gondwana in the Late Jurassic - Early Cretaceous. This was followed by the opening, rifting and drifting of the South Atlantic Ocean (Brown *et al*., 1995). The geological framework of the basin can be simply subdivided into two developmental phases: a syn-rift phase (Late Jurassic – Early Cretaceous) and a post-rift phase (Late Cretaceous – Tertiary) (Brown *et al*., 1995).

This syn-rift phase led to the formation of graben and half grabens. These grabens tend to trend almost parallel to the present day margin. The sediment belonging to the syn-rift phase is made up of mostly siliciclastic and lacustrine strata, deposited during the Late Jurassic to Early Cretaceous period (Brown *et al*., 1995). There is also a substantial amount of volcanic sequences in the syn-rift phase. These volcanic sequences were deposited to the east of the marginal ridge and in isolated half-grabens located on the middle and inner shelf (Paton *et al*., 2007).

The breakup of Gondwana played an important role in controlling the rift geometry and the development of the Indian and Atlantic Oceans (Watkeys, 2006). The five steps outlined below by Watkeys (2006) summarise the stages of the Gondwana breakup, which are critical in understanding the formation of the Orange Basin.

1. The first stage is represented by no real continental separation, even though rifting began. This occurred between 180-175 Ma, when Karoo volcanism began.
2. Stage two occurred between 175-155 Ma and included microplate rotation, which was a result of strike slip movement along the Gastre Fault-Falkland-Agulhas Fracture Zone (GFFAFZ). This linked the Gastre Fault System and the Agulhas Falkland Fracture Zone and led to the stretching of the proto-Pacific Ocean.

3. Stage three (155-135 Ma) represents the splitting of Gondwana into an east and west Gondwana due to the strike slip movement occurring along a connected fracture system (GFFAFZ). According to Dingle *et al*. (1983), this movement could be the reason for the initial northward rifting that occurred along the western coast of Southern Africa. This is evident by the formation of the Orange and Walvis Basins separated by the Lüderitz Arch.
4. The main event that occurred during stage four was the positioning of the continental rift-zone over the Tristan da Cunha plume. This developed under the South American Parana Basin during the period when Africa separated from South America (Turner *et al*., 1994). The plume intruded through the weaker crust and kickstarted the spreading of the sea floor between Africa and South America.
5. The final stage involved the final split in the South Atlantic. This split involved a triple junction jump to the southern continental part of the Agulhas Plateau. It was this final separation between Africa's and South America's continental crusts that allowed the entire Atlantic Ocean to combine.

The breakup between South America and Africa as discussed in stage three and stage four above, led to the formation of the western margin of Southern Africa. The Late Cretaceous post-rift phase is characterised by episodes of gravitational collapse of the margin (de Vera *et al*., 2010). This resulted in the basin being filled with the post-rift phase Cretaceous siliciclastic rocks, ranging in age from Late Hauterivian drift onset to Tertiary (Brown *et al*., 1995).

3.2 Regional geology

The development of the western margin of southern Africa forms the next crucial step in the ultimate formation of the Orange Basin. The western margin of South Africa is a rifted passive margin. Bott (1980) defined the formation of passive margins as a result of continental splitting, which may have followed an early pre-split graben stage of development.

According to Bott (1980), passive margins are formed by two major types of subsidence, namely; (i) a fault controlled graben subsidence followed by (ii) a flexural

down warping subsidence. These types of subsidence are described in four stages below (Bott, 1980):

1. The first stage involves a rift valley stage, but it isn't always present with the thermal uplift and graben formation before the breakup of the graben continent.
2. One of the results 50 Ma after the start of the splitting of the continents was the thermal effects of the split. These effects were heavily experienced in the form of pronounced thermal subsidence. Thermal subsidence occurs when conductive cooling of the mantle thickens the lithosphere, resulting in a decrease in the lithosphere's elevation.
3. This stage is referred to as the mature stage in which the passive development of the current Atlantic Margin occurred.
4. The final stage is regarded as the fracture stage when subduction began. This resulted in the end of the history as a passive margin.

The Orange Basin makes up a considerable part of the South African western continental margin and is defined by the extent and thickness of the post-rift sedimentary succession. Underlying the Orange Basin are basement grabens and half grabens, which are bound by the north-south striking normal faults (Barton *et al*., 1993).

These graben networks are divided into an inner marginal zone and central zone (Mutingh, 1993). The former zone is mainly filled with land-derived coarse-grained clastics, with a possible pre-rift unit inferred from onshore Karoo deposits. The latter zone is made up of thick successions, thought to be of fluvial and lacustrine nature. These successions overly a seaward-dipping sequence of reflectors. This sequence is a result of massive subaerial basaltic extrusion, which is linked with the continental breakup (Mutingh, 1993).

According to Brown *et al*. (1995), the Orange Basin underwent two phases of synrift as a result of the Gondwana Breakup:

1. The first phase included normal faulting during the early stages of the rifting of the Atlantic margin (Jurassic to early Cretaceous). These faults show

continuous rotation and displacement have produced grabens and half-grabens structures. The graben structures are trending in a north-south direction.

2. The second episode of deformation was a result of the extension of drift passive-margin phase sediments across the shelf. This drift phase started in the late Hauterivian and continues to the present.

The definition outlined by Bott (1980), along with the description of the stages above, matches many of the characteristics of the continental margin along the west coast of South Africa. These similar characteristics include; initial rifting in the formation of the basement grabens and half-grabens. This initial rifting was followed by an era of thermal sag when the deposition of the drift succession began and continued.

3.3 Depositional history of the Basin

The Orange Basin was fed by a major river system. Evidence of this can be seen in the location of the prominent deltaic depocentres, which are found near the mouths of the Orange and Olifants Rivers (Dingle *et al*., 1983). Interestingly, the Olifants River only contributed to the filling of the basin for about 13.5 million years, which then led to the Orange River being the only provider of sediment (Van der Spuy, 2003). It is possible for the sedimentary fill to be from the Jurassic period, but currently the oldest dated sediments are from the Hauterivian period. The sediments that have all penetrated are all continental, with some igneous lithologies in place (PASA, 2019).

The subaerial flood basalts, which were interpreted from hinge seismic seaward-dipping reflectors, are coeval and in parts inter-layered with continental to shallow marine sediments of the Barremian age (PASA, 2019). The Cretaceous sediments are siliciclastic and range from continental to deep marine in the east and west respectively. Compared to the Tertiary succession, which is made up of calcareous oozes and chemical sediments (PASA, 2019).

3.4 Sequence stratigraphy

Sequence stratigraphy is the study of the relationship of sedimentary deposits within a chronostratigraphic framework of repetitive or related strata. This sequence would be a conformable succession which is capped at its base and top by unconformities. These strata can be linked by either surfaces of erosion, deposition or their correlative conformities.
It normally includes splitting the sedimentary basin into singular sequences of deposition, which would be linked to changes in sediment supply and accommodation. The main objective of this is to recreate how sediments filled the basin, thus determining how the stratigraphy was formed throughout time and space.

A sequence according to Catuneanu (2006) is composed of a succession of deposition systems (system tracts) between eustatic sea-level changes.
System tracts are 3-dimensional facies assemblages that represent the sea-level cycle in the rock record. They are characterised on the basis of boundaries, position within the sequence and parasequence stacking pattern (Van Wagoner *et al*., 1988). They display changes in the depositional system across that boundary.

In a vertical succession, a sequence is laid out in the following order, starting from the bottom: sequence boundary (SB), lowstand systems tract (LSTT), transgressive surface (TS), transgressive systems tract (TST), maximum flooding surface (MFS) and highstand systems tract (HST) (Posamentier and Allen, 1999).

3.4.1 Sequence boundary (SB)

Sequence boundaries mark the beginning and the end of a depositional sequence. They can be identified as important erosional unconformities and their correlative conformities. They are a result of a drop in sea-level, which leads to the eroding of the subaerially exposed sediment surfaces of sequences that were deposited earlier (Catuneanu, 2002).

3.4.2 Lowstand systems tract (LST)

These are deposits that form after the start of a relatively high sea-level rise. It lies above the formation of a sequence boundary and is cut off by the transgressive surface above. The transgressive surface is a result of sediments onlapping onto the shelf margin. LST sediments often fill incised valleys, which were cut into the highstand systems tract (Posamentier and Allen, 1999).

3.4.3 Transgressive surface (TS)

This is the first maximum flooding surface after maximum regression. In shallower areas of the shelf, it is linked with erosion and represents the transition from non-marine to marine sedimentation (Nummedal and Swift, 1987). It separates the lowstand system tracts below from the transgressive systems tract above. The transgressive surface erosion are composed of lags, minerals (particularly glauconite concentrations) and cementation of the surface below (Baum and Vail, 1988).

3.4.4 Transgressive systems tract (TST)

This tract is located on the transgressive surface and is covered by the maximum flooding surface. It is made up of retrogradational sets of parasequences and it includes sediments that have accumulated from the start of the coastal transgression till the time of maximum transgression of the coast, just before renewal regression (Kamgang, 2013).

3.4.5 Maximum flooding surface (MFS)

This surface records the time of maximum flooding or transgression of the shelf. This surface also separates the transgressive and highstand systems tract. It records the deepest water facies in a sequence and is a representative of a change from retrogradational to progradational parasequences. Deposition on this surface is slow and deposits are mainly thin and fine-grained (Mitchum Jr, 1977).

3.4.6 Highstand systems tract (HST)

This systems tract forms part of the upper systems tract of a sequence stratigraphy. It occurs when sediment accumulation rates exceed the rate of a rise in the relative sea-level and an increase in accommodation forms part of the upper systems tract (Mitchum Jr, 1977). This systems tract is common on the shelf and is often represented by one or more aggradational to progradational parasequence sets and is capped at the top by the next boundary (Kamgang, 2013).

The types of geometries present in accommodation successions are used to differentiate the system tracts and sequences mentioned above. As the sediments are re-arranged, the characteristics of the sequences, system tracts, parasequences and beds will be identified as a result of changes in accommodation. This allows the sequence stratigraphic framework to discuss why sedimentary rocks display the characteristics and features they do. In turn, these characteristics can be used to explain the mechanisms associated with sediment accumulation and erosion.

The earliest sedimentation that occurred in the Orange Basin has been dated as Pre-Hauterivian and is thought to have started in the Kimmeridgian or Tithonian (~152 to 154 Ma) (Brown *et al*., 1995). The Orange Basin includes the stratigraphic record of lithospheric extension and rift tectonics throughout a completely evolved post-break-up setting. Figure 3.1 below, displays a good summary of the Orange Basin's stratigraphy (in terms of prerift, synrift, transitional, drift and tertiary to present day successions) and tectonic setting.

The sedimentary fill of the Orange Basin is thought to be a result of cyclic sea-level changes, thus a broad prograding sedimentary wedge has been observed that has been further divided by erosional unconformities. Four main depositional events, are observable in Figure 3.1, namely; Pre-rift, Synrift, Post rift (Transitional), Drift and Post-drift (Cretaceous and Tertiary).

The *pre-rift* phase is made up of Pre-Jurassic age basement rocks, ranging from low to high grade metamorphites in the south and granitic plutons and alkaline intrusives in the northern part (Broad *et al*., 2006).

These basement rocks are overlain by a Pre-Barremian synrift succession, which has formed a hinge line towards the basement. This succession is composed of complex grabens and half grabens. Synrift I consists of volcanic and alluvial rocks, followed by the synrift II with volcanic, alluvial and lagoonal rocks (Van der Spuy, 2003). This Pre-Barremian synrift succession is located between horizon T and 6At.

The *transitional* phase overlies the Pre-Barremian synrift phase and consists of the first marine incursions. It consists of an initial build-up of flood basalts and is then covered by alternating fluvial red beds and sandy marine deposits. These deposits were a result of successive transgression and regression of the sea-level (Muntingh and Brown, 1993). The transitional phase lies between the 6At1 and 13At1 horizons. The half-graben structures are filled with lacustrine rocks and volcanic intrusions.

The drift phase began between Hauterivian (130 Ma) and Mid-Aptian (100 Ma) times. This succession consists of Aeolian marine sandstones and shales, red continental sediments with inter-bedded lavas. During the Aptian period, the drowning of the margin occurred and underwent a thermal subsidence or eustatic change, which resulted in the deposition of organic-rich shales producing a source rock interval (Broad *et al*., 2006). These Aptian sandstones form the reservoir of the Kudu gas field offshore Namibia. The Barremian contains transitional to marine source rocks, and the basal part of the Aptian is marked by an anoxic black-shale event (Van der Spuy, 2003). The drift stage is characterized by turbidite sedimentation consisting of basin-floor fan, slope fan, and turbidite units containing mainly clastic shale, siltstone, and sandstone (Mutingh, 1993).

Cenozoic sediments were deposited as a well-developed wedge of siliciclastics. These deposits increased in thickness from 200 m on the shelf to 1500 m basin ward. This succession was formed by organic and chemical sedimentation consisting of terrigenous sediment, with hardly any continental sediment supply, apart from the ride and fall of sea levels (Broad *et al*., 2006).

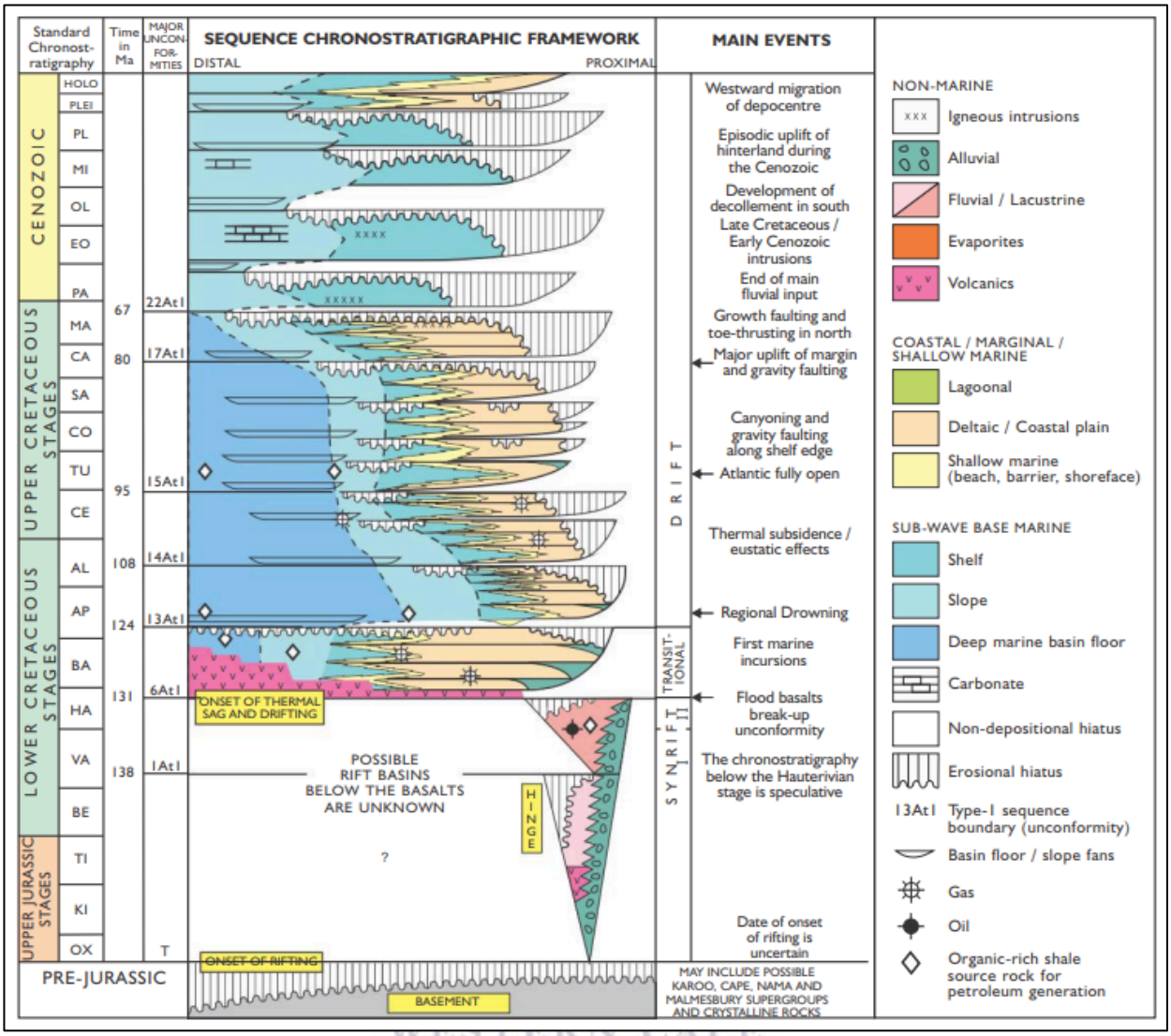

Figure 3.1 Chronostratigraphy of the Orange Basin (PASA, 2019).

3.5 Petroleum system of the Orange Basin

A petroleum system defined by Magoon and Dow (1994) is a genetic relationship, which links the source rock to all the generated oil and gas. In order for a petroleum system to exist, all the necessary geological elements need to be present to allow petroleum deposits to form and accumulate. Figure 3.2 below, provides a favourable summary profile of the petroleum system that is present in the Orange Basin.

A geological model was created by Brownfield (2016) for the assessment of conventional oil and gas in the Orange River Coastal Province and is summarised below, which summarises the petroleum system described below in the Orange Basin:

1. Hydrocarbons formed from Barremian-Aptian and Cenomanian-Turonian Type II marine source rocks during progradation. Possibly 7000 m of sediment was deposited during this drift-passive-margin stage
2. The actual generation most likely would have started in the Late Cretaceous continuing to the present day. The Early Cretaceous Type I lacustrine source rocks possibly led to the hydrocarbons being generated in the Early Cretaceous.
3. The hydrocarbons migrated into Cretaceous and Cenozoic sandstone reservoirs. These reservoirs included deltaic, nearshore marine sandstone, continental margin, slope turbidite sandstones and basin-floor fans.
4. The structural hydrocarbon traps include growth-fault-related structures, rotated fault blocks within the continental shelf. This is compared to the stratigraphic traps, which include deep-water fans, turbidite sandstones, and slope truncations. These stratigraphic traps are occur on the modern day shelf and paleoshelf edge.
5. The Cretaceous and Cenozoic mudstone and shale rocks make up the major reservoir seals.

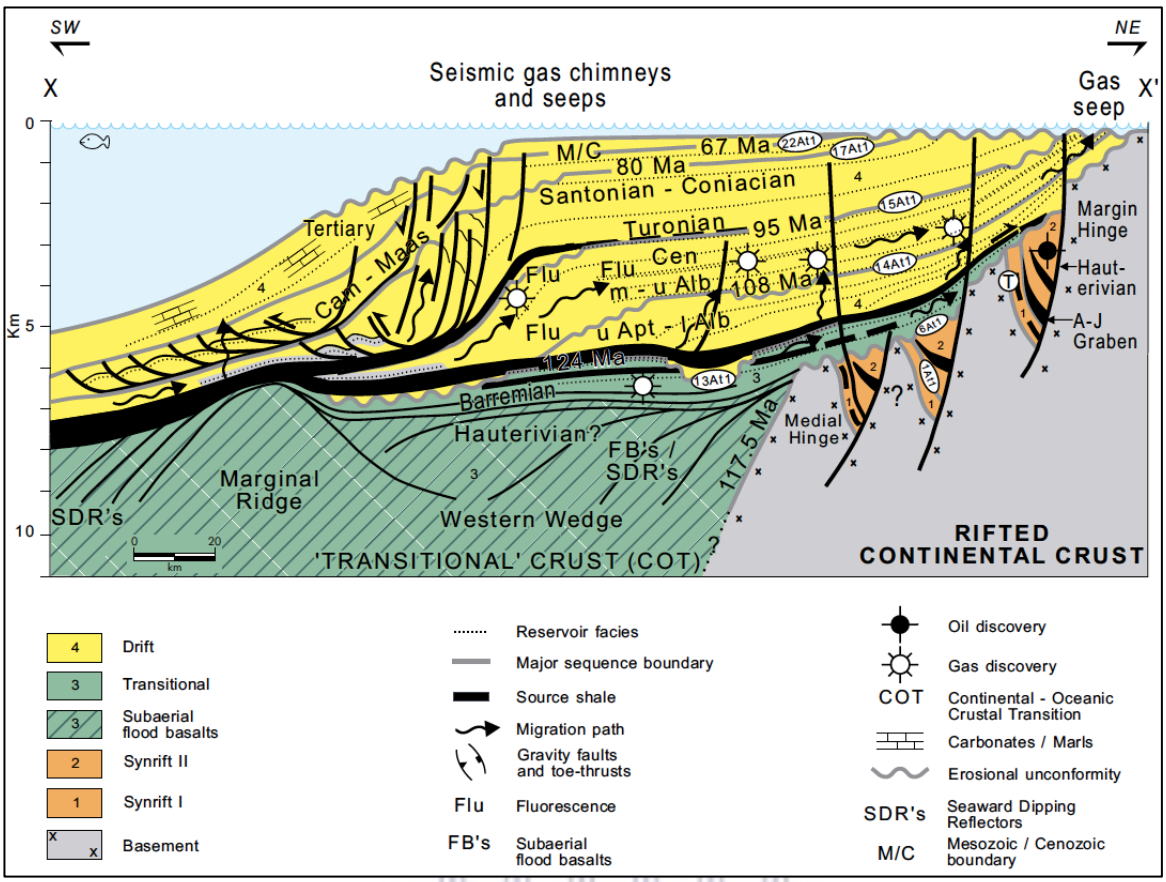

Figure 3.2 Displays a cross profile of the petroleum system elements of the Orange Basin (Jungslager, 1999).

3.5.1 Source rocks

Source rocks are fine-grained sedimentary deposits, formed in anoxic environments, containing a significant amount of organic matter. Source rock generates and releases enough hydrocarbons to form an accumulation of petroleum. Shale contains 90% of all organic matter found in sediments and thus is found to be a brilliant source rock. Shales can also act as seals depending on their position in the stratigraphic column in the reservoir (Frank *et al*., 2008).

In the Orange basin, a number of source rocks have been identified and are known to occur in the shaly Cretaceous formations in the synrift and drift sediments. In the synrift sediments of the separated A-J graben, a Hauterivian oil-prone lacustrine shale is found, with a the total organic carbon (TOC) greater than 10%. The presence of this oil-prone shale deposit suggests it may be possible for similar organic-rich shale intervals to be present in other rift grabens along the continental margin. There have

also been regional correlations with this interval along the South American margin (Jungslager, 1999).

During the period of the Barremian to Early Aptian, quick deepening resulted in the deposition of Type II marine-transitional source rock in the Aptian anoxic basin (Van der Spuy, 2003). This sequence relates to a transitional phase between syn-rift and drift. It was during this time period that the highest quality of source rock was deposited. This source rock is known to be oil-prone (TOCs of up to 25%) and has a potentially large lateral distribution, which is evident from the exploration wells and Deep Sea Drilling Project site 361 (Herbin *et al*., 1987). Van der Spuy (2003) proposed that this source rock most likely contributes to the Ibhubesi and Kudu Gas fields.

3.5.2 Reservoir rock

Reservoir rocks are rocks that are both permeable and porous, occur in a suitable stratigraphic position and allow the containment and yielding of oil and gas that is suitable for commercial use. The most important property of a reservoir rock is its porosity, but the permeability is important too, as it is used to determine the reservoir's effectiveness (Williams, 2018). Porosity and permeability are at their highest when the rock has been deposited, and diminish considerably as compaction occurs. Typical reservoir rocks are coarse-grained sandstones and fractured fine-grained carbonates.

In the Orange basin, the reservoirs are Late Jurassic and Early Cretaceous syn-rift and linked with grabens and half-grabens in the deeper parts of the offshore A-J graben (Jungslager, 1999). The reservoirs in the syn-rift areas include fluvio-deltaic and lacustrine sandstone, interbedded with conglomerates in the shelf. This is compared to the drift-passive margin reservoir, which include deltaic and turbidite sandstone (Barton *et al*., 1993).

The dominant oil-bearing reservoir is located within the Albian successions. This reservoir is made up of thick and thin bedded clay, silt and sand sequences (3 m – 70 m), along with thin and shaly beds (Muntingh and Brown, 1993). The beds in these

sequence are characterised by being laminated and have bioturbated mudstones to massive planar cross-bedded sandstones that coarsening upwards (Mutingh, 1993).

In the Kudu Gas field, stratigraphically trapped Barremian aeolian sandstone and Albian-Cenomanian sandstone act as gas reservoirs. Presently, the best reservoir properties and gas flow rates are located in the Middle Albian to Cenomanian aged fluvial channel sandstones of the Ibhubesi gas field (Jungslager, 1999). However, it is possible for potential oil-bearing reservoirs to occur in deep water turbidite sandstones. These deposits would connect with major syn-sedimentary structures and may occur in the oil window of Aptian source rocks (Jungslager, 1999).

3.5.3 Traps

Traps are the geometric arrangements of strata that allow the accumulation of hydrocarbons in a reservoir (suitable for commercial purposes) without the hydrocarbons migrating. It includes the reservoir rock containing the oil and gas, a seal or multiple seals that prevent petroleum leakage. There are two main classifications of traps:

- Structural traps require the secondary movement of strata to create post-depositional structures. These structures are often formed by the shifting of fault layers along the fault plane. Anticlines and faults are examples of structural traps (Kamgang, 2013).
- Stratigraphic traps are formed by primary depositional changes (facies changes and pinch-outs), where a reservoir is cut off by an impermeable horizontal layer and does not require structure. They are lithological traps due to the presence of impermeable layers above and below the reservoir (North, 1985).

In the Orange basin, the structural traps include growth-fault-related structures and and rotated fault blocks located on the continental shelf. This is compared to the stratigraphic traps, which include deep-water fans, turbidite sandstones and slope truncations. The stratigraphic traps are located on the paleoshelf edge and the present-day shelf (Muntingh and Brown, 1993). An example of a stratigraphic trap can be found in the Kudu field, which forms at the feather edge of the seaward dipping

reflector sequence. This trap consists of medium-grained aeolian and fine to medium-grained fluvial sandstones, which are interconnected with basalts and volcaniclastics (Africa, 2016).

3.5.4 Seals

Seals are typically impermeable ductile strata, which are commonly shale or evaporites, hindering the further migration of hydrocarbons. In the Orange basin, the Early Aptian shales are the major source rock and the regional seal, which stops the migration of continental carrier beds below (Jungslager, 1999). Unlike the Early Aptian shale, the Turonian Stage (part of the Cenomanian-Turonian boundary) forms part of both the regional source rock and seal. This seal prevents the movement of the shelfal carrier beds below (Jungslager, 1999).

4. CHAPTER 4: Methodology

This chapter was apportioned into three sections, namely, seismic, petrophysics, and modelling. This separation helped with the coherence of the study and aided in the understanding of the different methods applied to deliver the results.

Considering this study as multi-disciplinary, a multi-faceted approach is taken, which is described in the flow chart presented in Figure 4.1. This flow chart summarises the order in which the necessary steps were taken to successfully complete this study. Beginning with data quality control, the methodology splits into two streams (geophysical and petrophysical analyses). After the analyses, the two sets of data are brought together to build the final reservoir characteristic models.

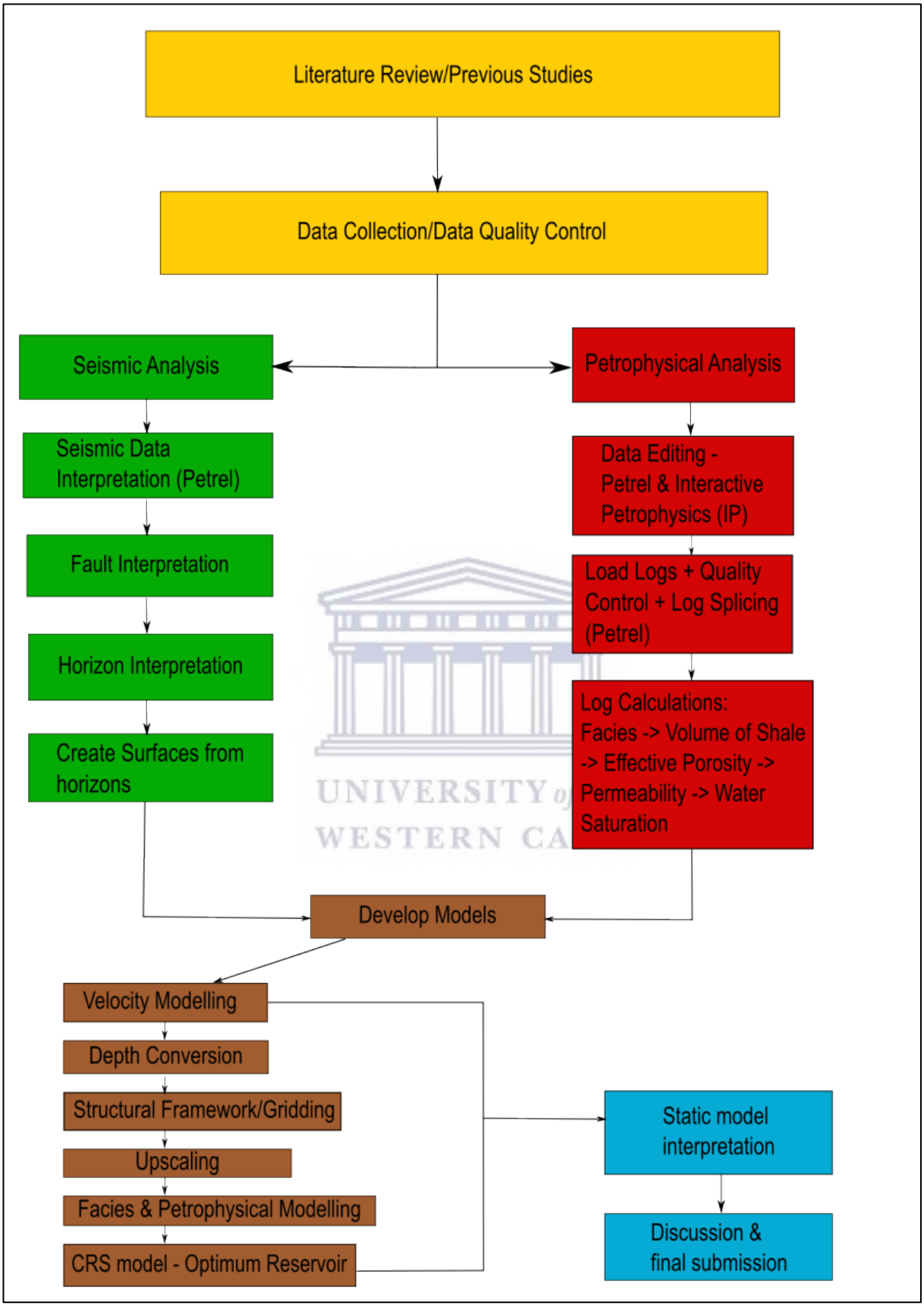

Figure 4.1 Flowchart of methodology

4.1 Data collection

Data used in this study (well data and seismic data) were provided by the Petroleum Agency of South Africa.

4.1.1 Data type

- Geophysical data
  - ⇒ The geophysical logs that were used are digital wireline logs LAS format: gamma ray log, density log, neutron logs, sonic logs, resistivity logs and caliper log
- Seismic data
  - ⇒ 2-D seismic data in the SEGY format.

4.2 Software

Different kinds of software were used in this study. Schulmberger's Petrel 2018 as well as Interactive Petrophysics software (IP 4.1) were used for the seismic analysis, interpretation, and data conditioning of log files. Once conditioned, the log files were imported into the Interactive Petrophysics software for quality control, data editing, calculations of the log curves and interpretations. After performing the necessary calculations (porosity, volume of shale, water saturation, permeability), the logs were imported into Petrel for the upscaling of the logs as well as the modelling.

4.3 Petrophysical analysis

Petrophysics is the study of the chemical and physical properties of rocks and their interactions with contained fluids (Donaldson and Tiab, 2015). These properties can be measured directly from rock samples retrieved from boreholes as cores or they can be derived from electronic measurements, which are carried out in the borehole during or after the well has been drilled. The petrophysical properties that are of important interest, such as permeability, porosity, volume of shale and water saturation are necessary to estimate the volume of hydrocarbons present in the well, which would

lead to the successful evaluation of the quality of the reservoir and determination of whether the reservoir is economically viable or not.

4.4 Wireline logs

Wireline logs are important because they are the main source of accurate information on the depths, apparent and actual thickness of lithological beds. They also produce information on the subsurface geology, such as formation boundaries, fluid content, and porosity, amongst others (Donaldson and Tiab, 2015). They can be based either on the visual inspection of samples brought to the surface (*geological logs*) or on physical measurements made by instruments lowered into the hole (*geophysical logs*) (SPWLA, 1975).

Interactive Petrophysics was used to plot the geophysical data, derived from the **.las* files. The basic petrophysical curves for well A-C1, A-C2 and A-C3 include GR, ILD, RHOB, NPHI, SP, DT and SFLU. These basic curves were used as the variables to calculate effective porosity, permeability, volume of shale and water saturation. However, the statistics of the results for GR, ILD, RHOB, NPHI, Effective Porosity, Permeability, Volume of Shale and Water Saturation for the three wells as a summary are discussed in this chapter.

The wireline logs are continuous evidence of the geophysical properties along a borehole. They are a result of wireline logging, which is a process that involves the insertion of a logging sensor or a combination of sounding probes into the drill collar. This is then lowered into the well bore by a cable and physical measurements are made. These physical measurements include electrical, nuclear, acoustical, thermal and dimensional.

Wireline logs are classified based on what measurable physical properties can be deduced from them.

- Classification based on operational principles:
  - ⇒ Nuclear or radioactive logs: gamma-ray (GR), density and neutron logs

⇒ Acoustic logs: sonic logs

⇒ Electrical logs: resistivity logs

- Classification based on their usage:
  - ⇒ Lithology logs: gamma-ray (GR) log
  - ⇒ Resistivity logs: induction, laterolog, micro resistivity logs
  - ⇒ Porosity logs: sonic, density and neutron logs
  - ⇒ Auxiliary logs: calliper, dip metre

Different logs are essential in calculating the different petrophysical properties. For example, the sonic and density well logs are used to create a synthetic trace, which is compared to real seismic data collected near the location of the well, while the gamma ray log and spontaneous log are used to calculate the volume of shale. These collections of logs will be used in this study and explained in more detail below.

4.4.1 Gamma-ray (GR) logs (*Lithological log*)

Gamma-ray logs measure the natural radioactivity of both parent and daughter isotopes belonging to the three main radioactive families (uranium, thorium and potassium) in rock formations. The log is a record of the rock's natural formation of radioactivity, and thus the log is used to identify lithologies and to derive the volume of shale in that formation, because shale has the strongest radiation signature compared to sandstones, dolomite and limestone (which have the weakest radiation signature) (Rider, 1996).

The log reflects mainly the clay content because clay contains the radioisotopes from all three families. Potassium is found in high concentrations in evaporates, carbonates and in low concentrations in feldspars in sandstones. Thorium, on the other hand, is found in the detrital fraction of minerals (continental shale, some beach sands and placers). This is compared to uranium, which is found in clay minerals containing organic matter, clay particles and adsorptive material (amorphous silica, alumina and coals) (Serra and Sulpice, 1975). It is possible for volcanic ash, potassium feldspars, granite wash and some salt-rich deposits, that contain potassium to give a reasonable

gamma-ray reading. Sandstones that are shale-free and carbonates that have low concentrations of radioactive materials show low gamma-ray readings.

Gamma ray units are measured in American Petroleum Institute (API). High gamma ray values of about 100 API are mostly encountered in shales. Clean reservoirs normally have low gamma ray values (15 to 25 API units) (Bigelow, 2002). Using these key characteristics, a filter can be added to the gamma ray log to identify where there is sandstone compared to shale. By using the gamma-ray log as a guide, the lithology and potential reservoir zones in the correct stratigraphic position can be identified. A baseline can also be created using the gamma-ray histogram plot. The baseline is used to detect and identify clean sandstone and shale.

4.4.2 Neutron logs (*Porosity log)*

A neutron log measures the number of neutrons scattered from the formation after it has been exposed to a neutron source. These neutrons are expelled from a radioactive source, which is held against the borehole wall. Neutrons lose energy when they crash into an atomic nucleus and lose most of their energy when the nucleus has a similar mass to the neutron (hydrogen nucleus). The neutron is slowed to thermal velocity after sufficient collisions have taken place and is then captured or scattered by elements in the formation, releasing a gamma ray. The more hydrogen is in the formation, the less the neutrons must travel. Thus, the number of neutrons or released gamma rays is related to the amount of hydrogen in the formation (Baker *et al*., 2015).

Neutron logs thus measure the concentration of hydrogen in a formation. The concentration of hydrogen in the formation indicates the level of porosity in that formation. Thus, when the pores are filled with gas rather than oil or water, the neutron porosity will be lowered. This is because there is less concentration of hydrogen in gas compared to oil or water (Bigelow, 2002).

When the neutron log is used in combination with the density log, it can be used for hydrocarbon identification. In this study it was used to identify gas. The main use of the neutron log was to distinguish between oil, water and gas saturations (the porosity will be low when gas is measured).

4.4.3 Density log (*Porosity log)*

The density log measures the bulk density of the formation and produces a continuous record of the formation's bulk density. The main purpose of this log is to determine a value for the total porosity of the formation and hydrocarbon density, but it is also useful in the identification of the presence of gas-bearing formations and the identification of evaporites. In combination with the neutron log, it is a useful tool as an indicator of lithology and minerals, as well as to identify overpressure and fracture porosity. If the matrix density is constant, the density of coal and associated rocks is an inverse function of the porosity (Flores, 2014).

The formation density tools are used as induced radiation tools, because they expose the formation with radiation and measure how much radiation returns to the sensor. The gamma ray sensor that measures the gamma ray count at the surface is an inverse function of the density of the coal or associated rocks. Thus, the more gamma rays that are absorbed in the denser rocks, the less is detected by the sensor. Coal generally has a low density (0.7-1.8 g/cc), compared to adjoining lithologies. This makes the density tool very useful in identifying coal beds (Flores, 2014).
The rate of absorption and intensity of the backscattered rays is dependent on the number of electrons (electron density) the formation contains, which is related to the density of the materials. Denser materials have more electrons per unit volume, which collide with the gamma rays and lose energy. Therefore, more energy is absorbed in denser formations. In lighter materials with lower electron density, a greater number of gamma rays reach the detectors and are converted to bulk density in the log (Kamgang, 2013).

The density log was used for the identification of hydrocarbons. Identifying spikes in the data allowed for the determination of what hydrocarbon was present (oil or gas).

4.4.4 Sonic log (*Porosity log)*

Sonic logs are a continuous record against depth of a specific time required for a sound wave to travel across a given distance of formation next to the borehole. The

sonic log changes depending on the lithology, rock texture and porosity. Thus, the sonic log works well to identify subtle changes in rock textures in both shales and sands. Sonic logs were used to determine the porosity of liquid-filled pore spaces. When used in combination with the density, it was used to produce the acoustic impedance log, which is the initial step in creating a synthetic seismic trace.

The sonic tool is made up of two receivers and one transmitter. Once the transmitter becomes energised, the sound wave enters the rock formation from the mud column and travels through the formation (mud column) back to the receiver. This travel time (formation velocity) is equivalent to the distance between the two receivers. The sonic tool compensates for changes in the borehole size or if the tool tilts.

4.4.5 Resistivity log (*Electrical log*)

Resistivity log is the oldest type of well log, dating back to 1927, when it was first used in formation evaluation by Conrad, Marcel Schlumberger and Henri Doll. It is the measurement of a formation's resistivity, which is the formation's resistance to allow the flow of an electric current. This can be carried out directly or indirectly, making use of resistivity tools or conductivity tools respectively.

Most rock materials are insulators, but their trapped fluids are conductors, except for hydrocarbons, which are infinitely resistive. If a formation is porous and contains salty water, the total resistivity would be very low (Kamgang, 2013). However, if that same formation contained hydrocarbons, the total resistivity would be very high. It was because of this nature that resistivity logs were effective in determining if pores are filled with hydrocarbons or not. Resistivity logs can also be used in addition to other logs to determine the lithology, texture, facies and overpressure of a formation.

4.5 Log calculations (Porosity, volume of shale, permeability etc)

The results from the basic log functions (NPHI, RHOB, ILD and GR), were used to determine the volume of shale, effective porosity, permeability and water saturation.

The calculated logs were then exported from IP and imported into Petrel to be used to build the final models.

4.5.1 Volume of Shale

The volume of shale is defined as the volume of shale per unit volume of reservoir rock. This calculation is important as it is an indicator of reservoir quality, as a lower shale volume would indicate a better reservoir. The volume of shale was calculated using the gamma ray log, due to shale's radioactive nature, using the following formula;

$$IGR = \frac{GR\ (log) - GR\ (min)}{GR\ (max) - GR\ (min)}$$

Where;

IGR = Gamma-ray index

GR (log) = Gamma-ray reading from log

GR (min) = Gamma-ray sand line

GR (max) = Gamma-ray shale line

Using the IGR value, the volume of shale can be calculated using (Steiber, 1970);

$$Vsh = \frac{IGR}{3 - 2\ (IGR)}$$

Where;

Vsh = Volume of shale

4.5.2 Porosity

The total porosity curve was derived from the combination logs of the neutron and density curves. The effective porosity was calculated from the subtraction of the total porosity from the volume of shale.

4.5.3 Permeability

The permeability calculation used in this study is based on the Timur model. Similarly to other permeability models, such as Morris and Biggs (1967), Timur (1968) proposed a model which uses porosity and irreducible water to determine the porosity. However, Timur's model is different in the sense that the fluid type in the reservoir does not have to be differentiated. The equation is;

$$K = a \times \left(\frac{(\phi^b)}{(Swir)^c} \right)$$

Where;

K = Permeability

Φ = Porosity

Swir = Irreducible Water

a = 8581 (constant)

b = 4.4 (constant)

c = 2 (constant)

4.5.4 Water Saturation

Before calculating the water saturation, the water resistivity (Rw) was determined. This was the resistivity value of water, which is uncontaminated by the drilling mud. The drilling mud causes the saturation of the porous formation to occur. Once Rw is calculated, the Archie model was used to calculate the water saturation. This model based on the fact that the water saturation of rocks can be related to the resistivity of rocks (Archie, 1942). The formula explains that when there is increasing porosity, the water saturation will decrease for the same resistivity as in "clean" rock. The formula is displayed as;

$$Sw = (\frac{a}{\phi^m} \times \frac{Rw}{Rt})^{\frac{1}{n}}$$

Where;

Sw = Water Saturation

a = Lithology factor

Φ = Porosity of the formation

m = Cementation factor

Rw = Water Resistivity

Rt = Deep resistivity of the formation

n = Saturation exponent

This model is used best for clean sands. These sands have a porous medium and a non-conductive matrix. This is important as the only conductive variable in the formation should be the electrically conductive fluid (brine). The Archie model was used because only resistivity tools were run. However, the Timur method for permeability and the Archie Method for water saturation proved to be the most effective.

4.6 Seismic analysis

A total of nine seismic lines were provided by PASA for the study area. However, once they were correctly positioned, only six of the nine seismic lines plotted in an area to be suitably analysed contributed to the study area, as displayed in Figure 4.2..

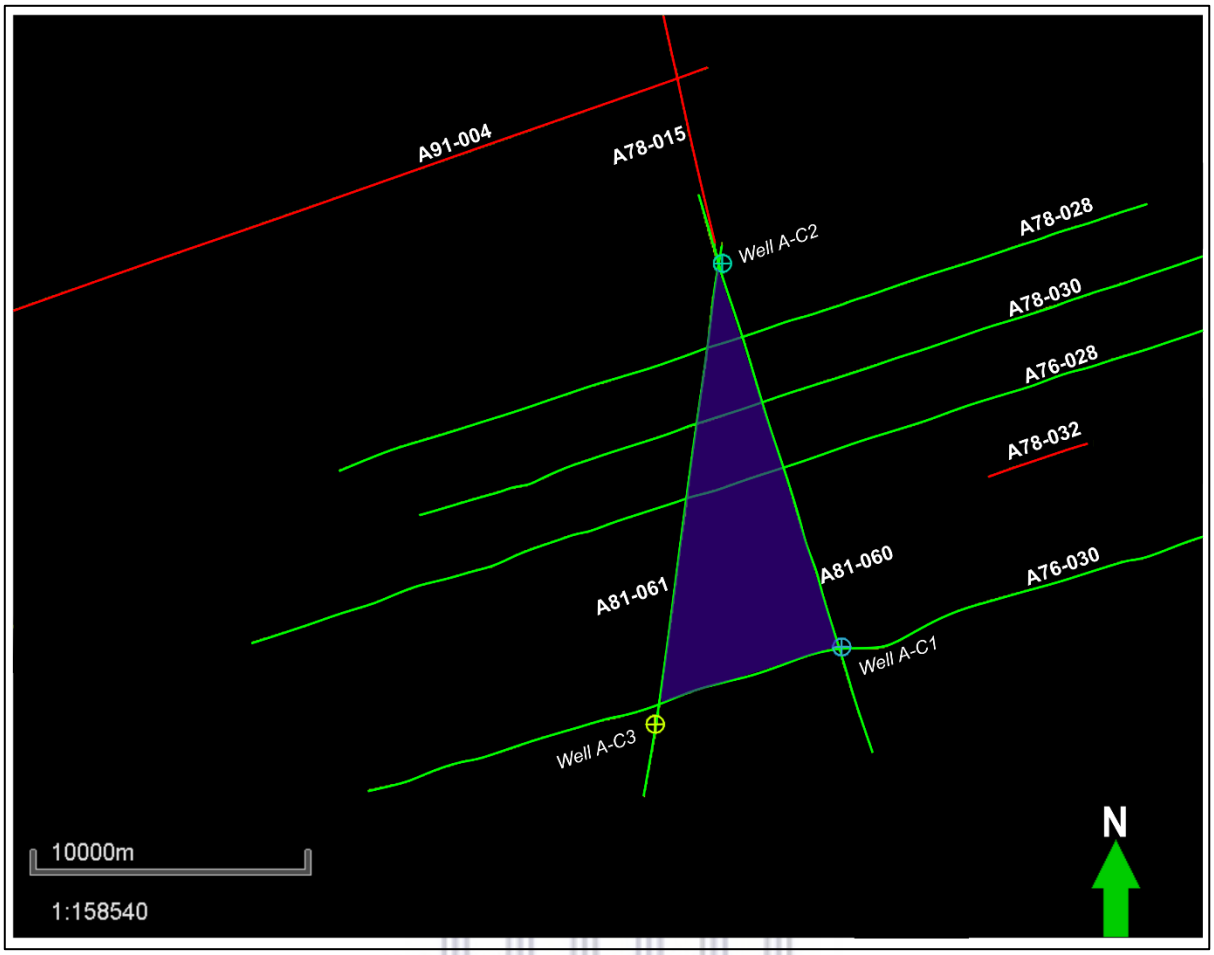

Figure 4.2. Displays the nine seismic lines correctly positioned.

Before interpreting the seismic data, well-to-seismic were carried out. Well seismic ties allow the well data, which is measured in units of depth, to be compared to seismic data, which is measured in units of time. This is critical to accurately calculate and interpret subsurface properties. The addition of check shot data allows the seismic data to be positioned at the correct depths. This is because the check shot data is the measurement of travel time between the surface and any given depth. The horizon tops in a well with specific reflections in the seismic data can be identified once the check shot data is processed (Figure 4.3).

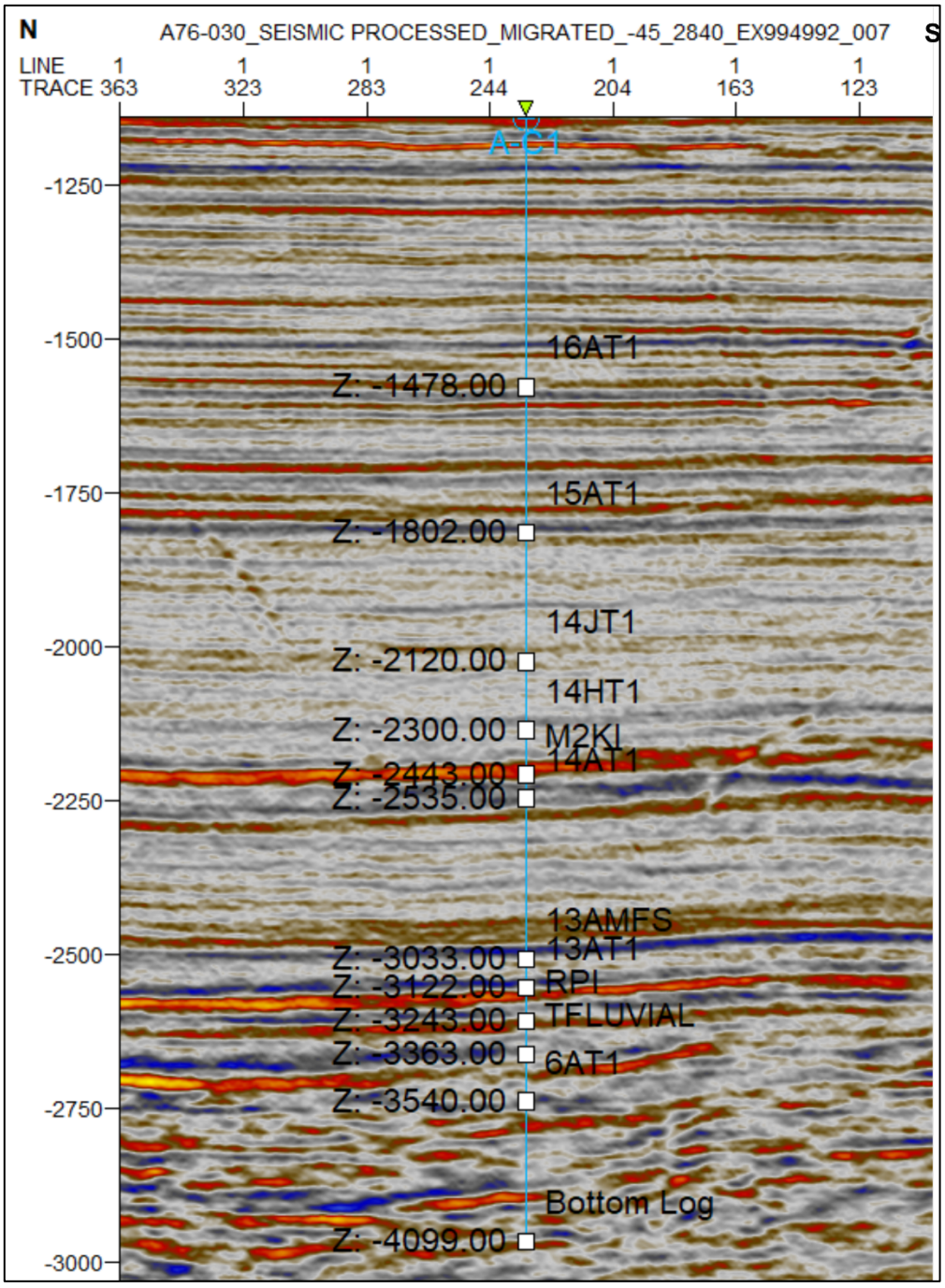

Figure 4.3. Displays the check shots, well tops and depths in well A-C1.

The gamma ray log was first added to the three wells on Petrel. It was analysed to determine if there were potential target areas in the wells. Once the potential target areas were identified, and the reservoir bounding sequences were picked (Figure 4.4).

The well tops were used to mark the boundaries of the two targeted areas. The well tops were used as they are consistent throughout the various wells and study area.

This is important, because the depths of the picked horizon would change as you move seaward, thus the bounding horizons couldn't be picked based solely on the depth of the depths at which the horizon is located. The two well tops for the first target area are M2KI and 13At1, which are the top and bottom boundaries, respectively. The second target area was bound by the TFLUVIAL sequence boundary at the top. The base was bound by the bottom log of A-C3, which was at a depth of 4150 m, relates to 3810 m on A-C1. The second target area was too deep to be identified in A-C2.

The horizons were picked using a combination of 2-D auto tracking and manual picking. The manual picking was used when the reflector was not clear nor was not identified with the 2-D auto tracking.

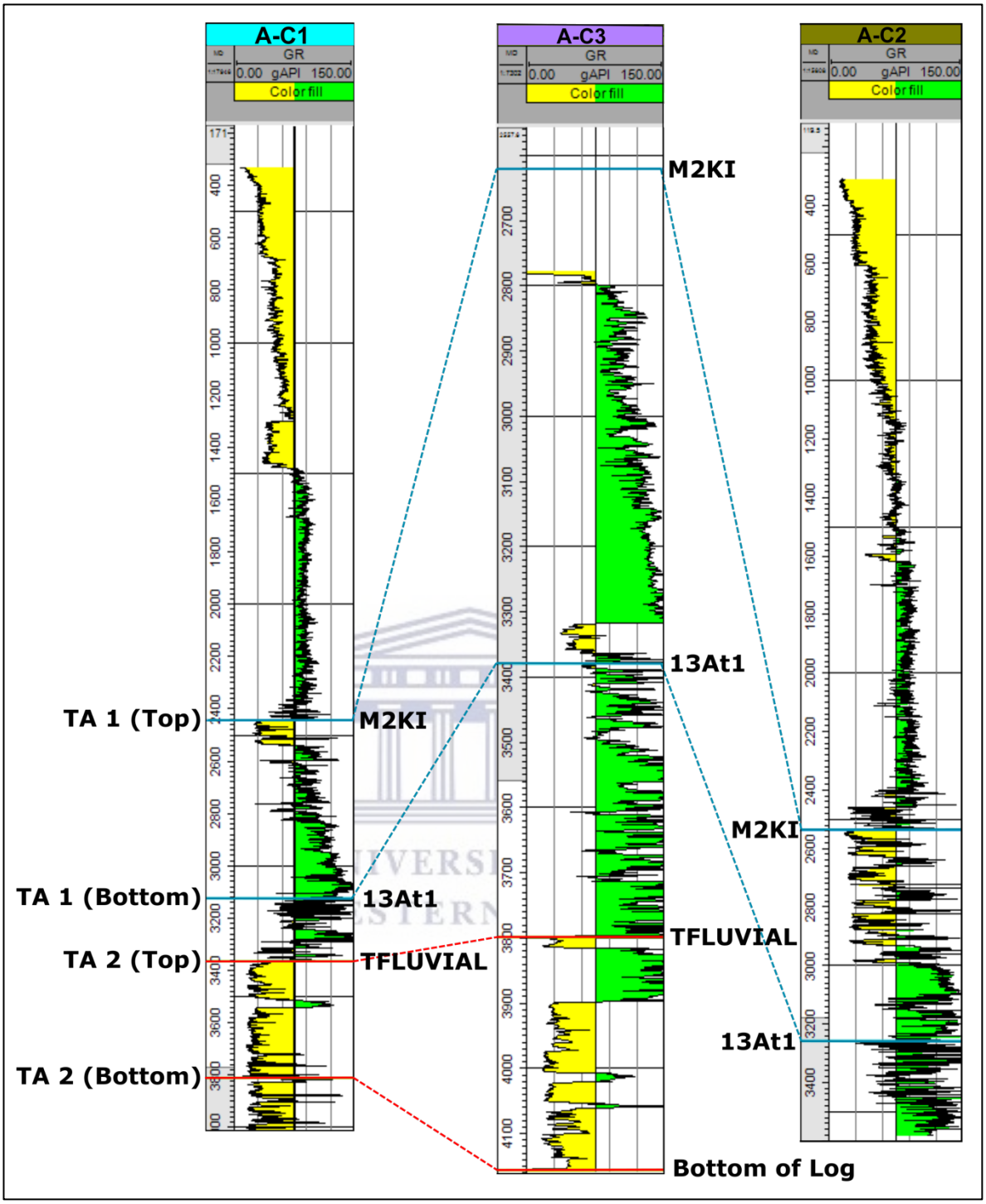

Figure 4.4. Displays the targeted areas (TA), identified using the gamma ray log on well A-C1, A-C2 and A-C3. The depth is in metres.

4.7 Modelling

Reservoir modelling incorporates geological information and information derived from a reservoir characterisation to generate a computer model of the potential of a

petroleum reservoir prospect. The reason for this is to improve the estimation of the petroleum reserves in the reservoir and improve the making of decisions regarding the development of the field, anticipating future production, adding additional wells and determine alternative reservoir management scenarios. There are two methods namely, static modelling and dynamic modelling. The former method is the one used in this study.

Static reservoir modelling incorporates seismic and data interpretation creates the structural framework, while the petrophysical log data creates the reservoir properties (Cunha, 2004). Furthermore, static modelling allows for any uncertainties to be calculated and risk assessments can be determined to aid in providing reliable estimations. This was carried out using Petrel.

4.7.1 Velocity modelling

A velocity model is the connection between time-to-depth conversion or depth-to-time conversion. This model describes the full sequence of velocities and corrections in a geological section and measures the time it takes between the surface and given depth to calculate the time depth relationship (Schlumberger, 2004).

A set of surfaces, zone definition for the velocity model and input parameters which would be a surface and data correction, such as the well tops, would be required to create these models. The linear velocity function used was:

$$\boldsymbol{V = V_0 = V_{int}}$$

Where:
$V = V_{int}$ (instantaneous velocity)
V_0 = Reference Velocity

The completion of the velocity models allows for the calculation of the interval velocities and the depth errors need to be fixed using the TDR (time-depth relationship).

4.7.2 Domain conversion

The reason for a domain conversion is to convert an object from one domain to another. In this study, it was used to convert from two-way time-to-depth once the velocity models were built. The objects that were converted were used in the building of the models, which included the target area boundaries, fault interpretations, well tops, surfaces, and seismic data. Once an object was converted, it could be displayed in either the two-way time domain or the depth domain.

4.7.3 Modelling framework

The surfaces that were created from the interpreted horizons from the seismic data and an outline of the triangulated study area were used to build the skeleton of the model. These horizons correlated to the sequence boundary horizons, which were linked to the top and bottom boundaries of the target areas. These surfaces formed the top and bottom of the 3-D model (Figure 4.5).

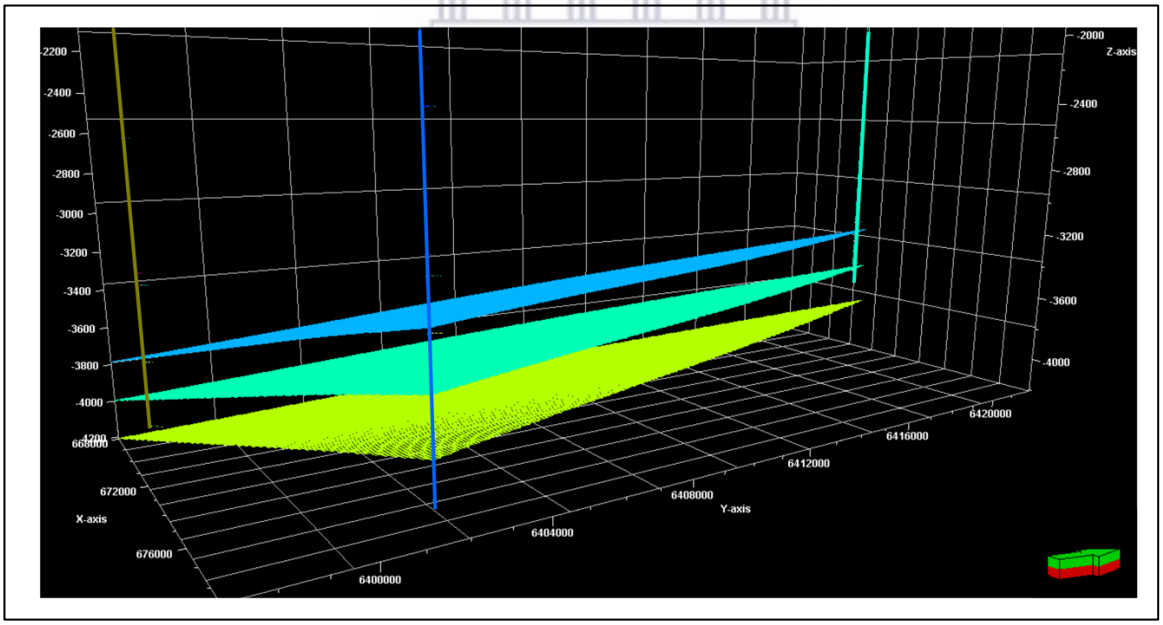

Figure 4.5. Displays the skeleton of the models.

After the skeleton of the model was built, the edges were added to the model. This can be seen in Figure 4.6. Before the model can be populated with various data from the well logs, the petrophysical data needs to be upscaled.

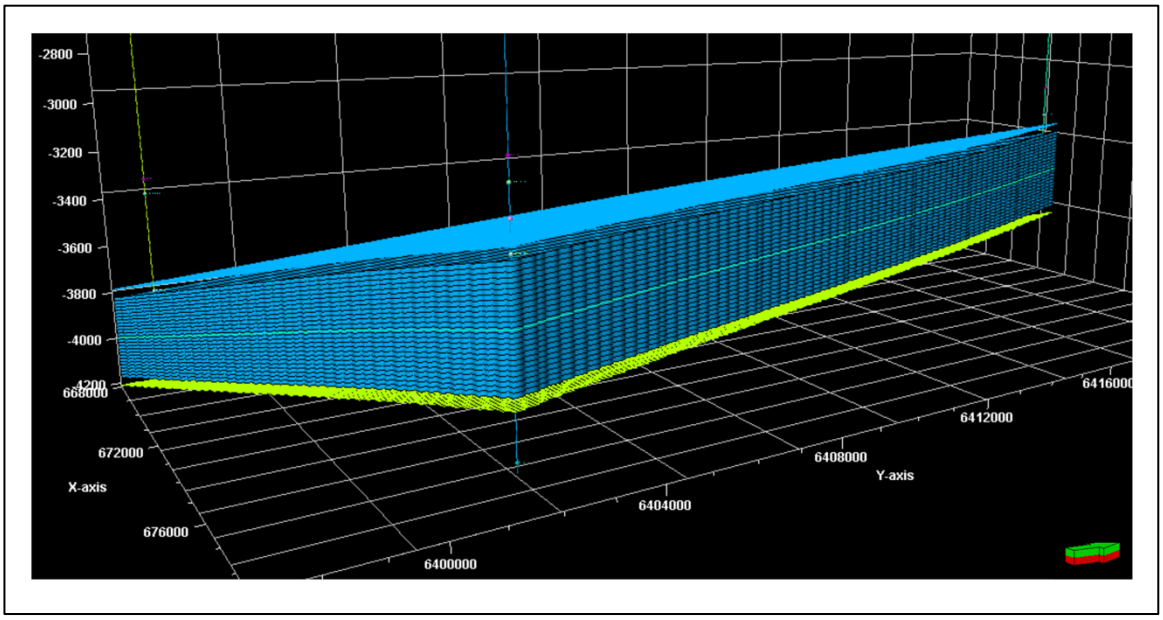

Figure 4.6. Displays the edges that have been filled around the skeleton.

Upscaling is a critical process to ensure the spatial prediction of the petrophysical data is correct. This is because, up to this point, the petrophysical data was only being displayed for the well log, thus it wouldn't be able to populate the areas outside the wells. This upscaling process involves the cells that pass through the well log in the seismic data, be given a value from the petrophysical data in the well log via the use of an algorithm.

This algorithm made use of the stochastic model, which made the values of the cells to be geo-statistically modelled, using the facies data as a bias factor. A part of the stochastic model is using Sequential Gaussian Simulations. This simulation is intended to add back some variability to correct for the smoothing effect of kriging. This results in a possibly better representation of the natural variability of the property (well log data) and creates a method for quantifying uncertainty (Nussbaumer *et al*., 2017). Once upscaling has been performed, the 3-D model can be populated with various data from the well logs, such as facies or water saturation.

4.7.4 Volumetric Calculations

After determining the Net Pay in each target area, the volume of hydrocarbons in each target area was calculated. It was previously determined that only gas was present in the target areas, thus the volume of gas and the gas water contact were calculated only.

The hydrocarbon pore volume is determined using the water saturation data, because pores that are not filled with water would be filled with gas. Thus, the following formula was used;

$$S_g = 1 - S_w$$

Where:

S_g is the gas saturation
S_w is the water saturation

5. Chapter 5: Results

This chapter is divided into three sections namely; seismic, petrophysics, and modelling. Once the gamma ray log was added to the three wells, it was analysed to determine if there were potential sandstone reservoirs in the wells. Once the potential sandstone reservoirs were identified, the bounding sequences of the reservoir were picked.

5.1 Seismic

A total of six seismic lines were analysed. Three of the seismic lines, namely: A76-030; A81-060 and A81-061, intersect at least one of the wells. These three lines were the first three to be interpreted. Using the gamma ray log, two target areas were identified in the study area (Figure 5.1). Target Area 1 is bound between the dark blue and the cyan coloured horizons, whereas Target Area 2 is bound between the purple and the orange coloured horizons. There were faults identified on the seismic lines. However, those were shallower faults and did not intersect any of the picked horizons. Thus, those faults were not included in Figure 5.1.

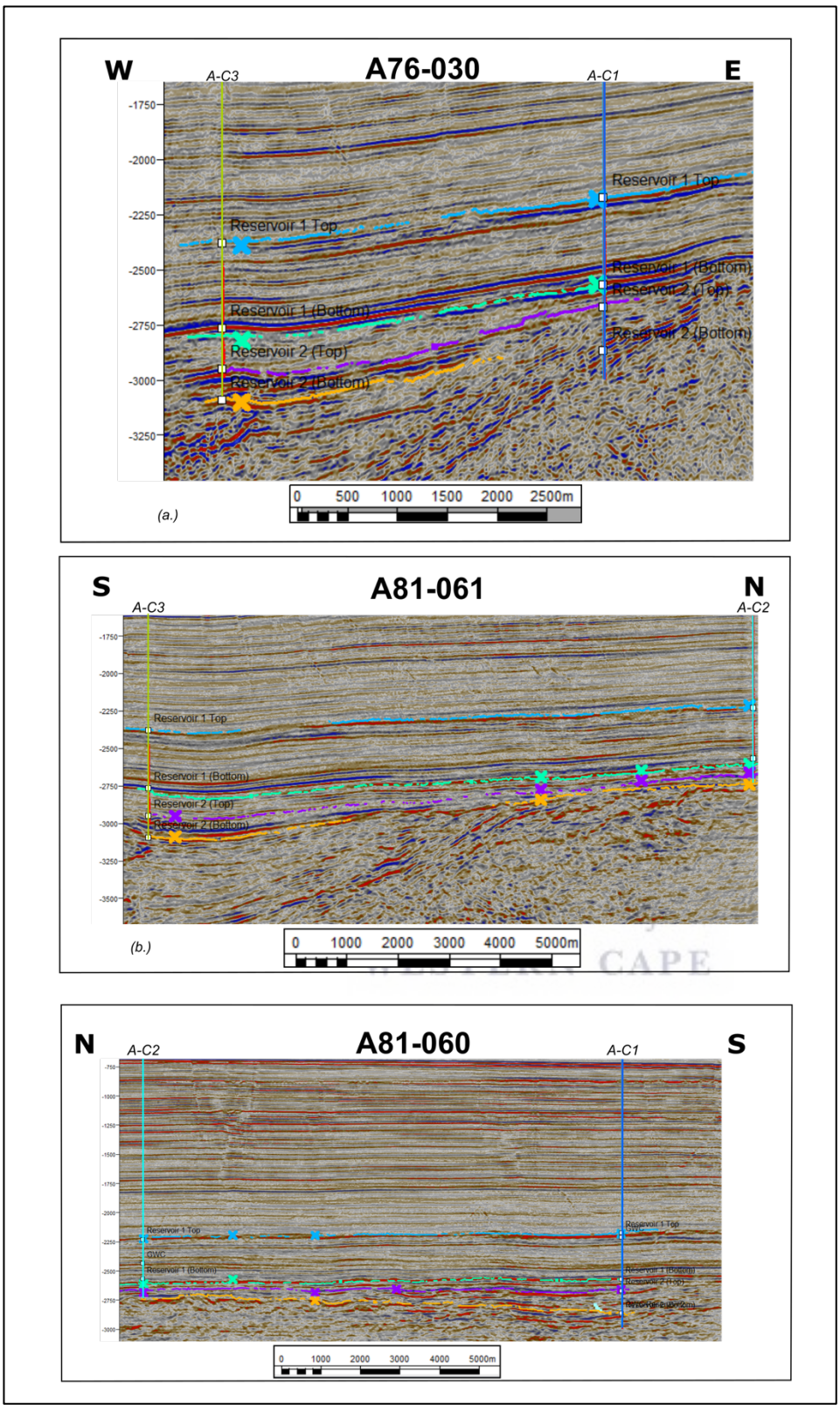

Figure 5.1. Displays the three main seismic lines, which form the perimeter of the study area. The "x" represents the horizon intersection on another seismic line.

5.2 Petrophysics

Well log data of the whole well are displayed below, to ensure the understanding of what the surrounding areas above and below the target areas look like. An analysis of this area will be discussed, identifying the trends in the data.

The gamma ray values were used to determine the two target areas, the sand-, silt-, shale- and basement facies in the well logs. The facies log formula was used to calculate the different facies percentages in the wells. Referring to Figure 5.2, A-C1 was analysed to have 33.9% of sand, 38.6% of silt and 12.6% of shale and 14.8% of basement. The basement facies was only found in the second targeted area in A-C1.

$$Facies = If(GR < x, 0, If(GR > y, 2, 1))$$

In relation to A-C1, GR is the gamma ray value, x is less than 60 and y is greater than 100. The sand, silt, shale and basement facies are represent as *0, 1*, *2* and 3, respectively.

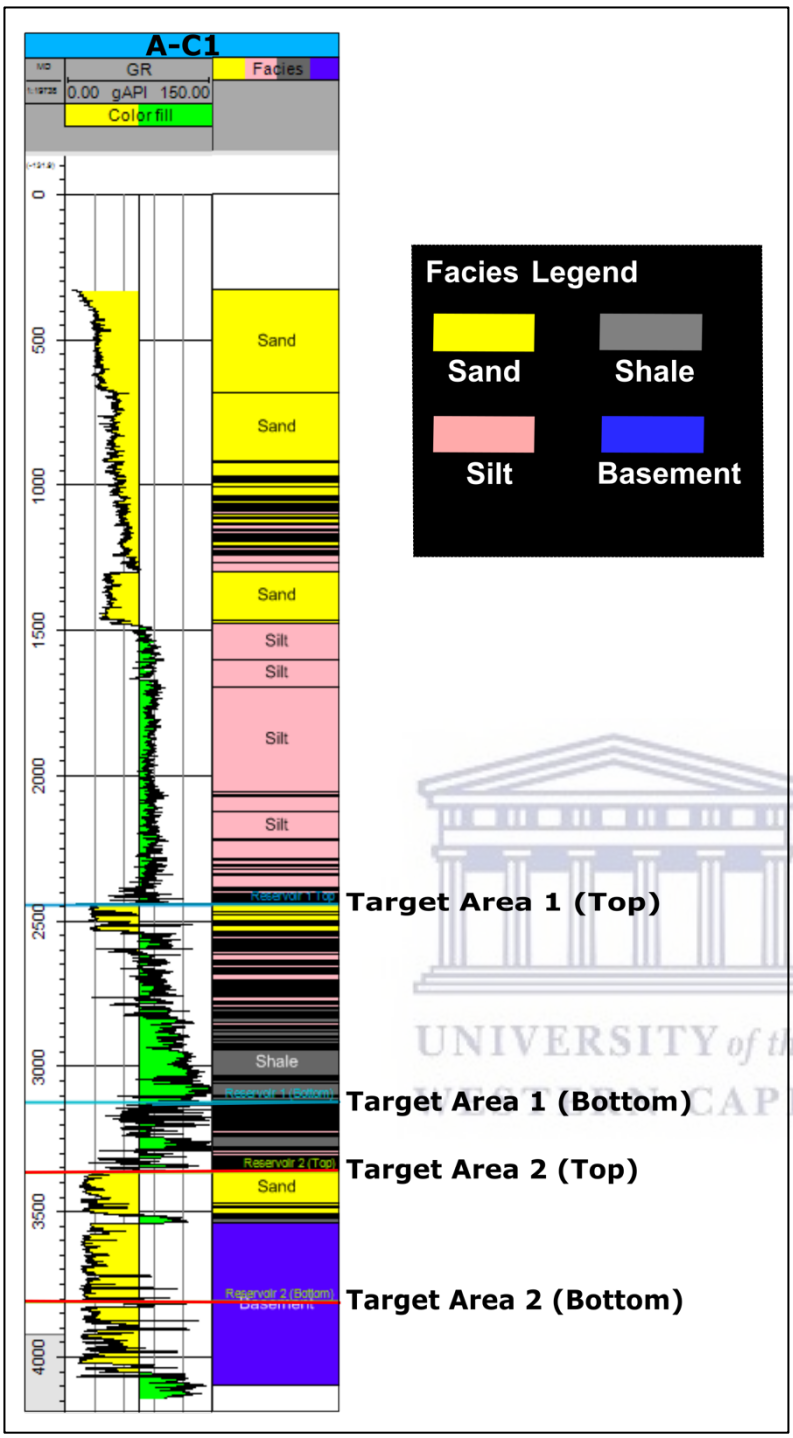

Figure 5.2. Displays the full well log of A-C1, which encompasses the potential target areas. The depth is in metres.

Compared to A-C2 (Figure 5.3), the facies was calculated to contain 15.1% of sand, 40.8% of silt, 40.7% of shale and 3.5% of basement. The 3.5% basement is at the bottom of the log and includes less than a 100 m of the log.

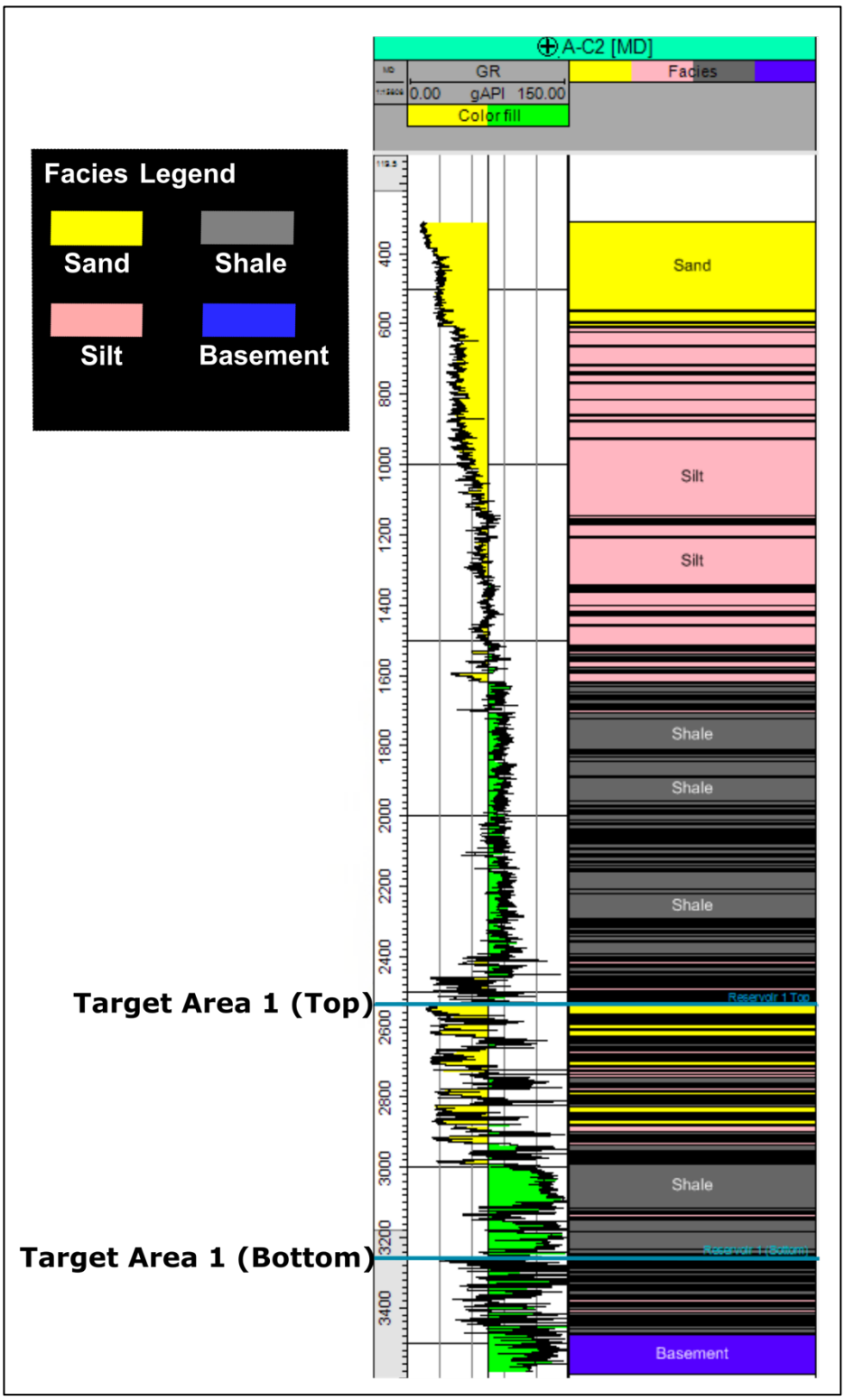

Figure 5.3. Displays the full well log of A-C2, which encompasses the potential target areas. The depth is in metres.

Lastly in A-C3, the x and y variables for the facies log formula were 70 and 130, respectively. This resulted in A-C3 containing 7.4% of sand, 42.1% of silt, 31.9% of shale and 18.5% of basement. Similarly to A-C1, the basement facies was only found at the bottom of the well (Figure 5.4).

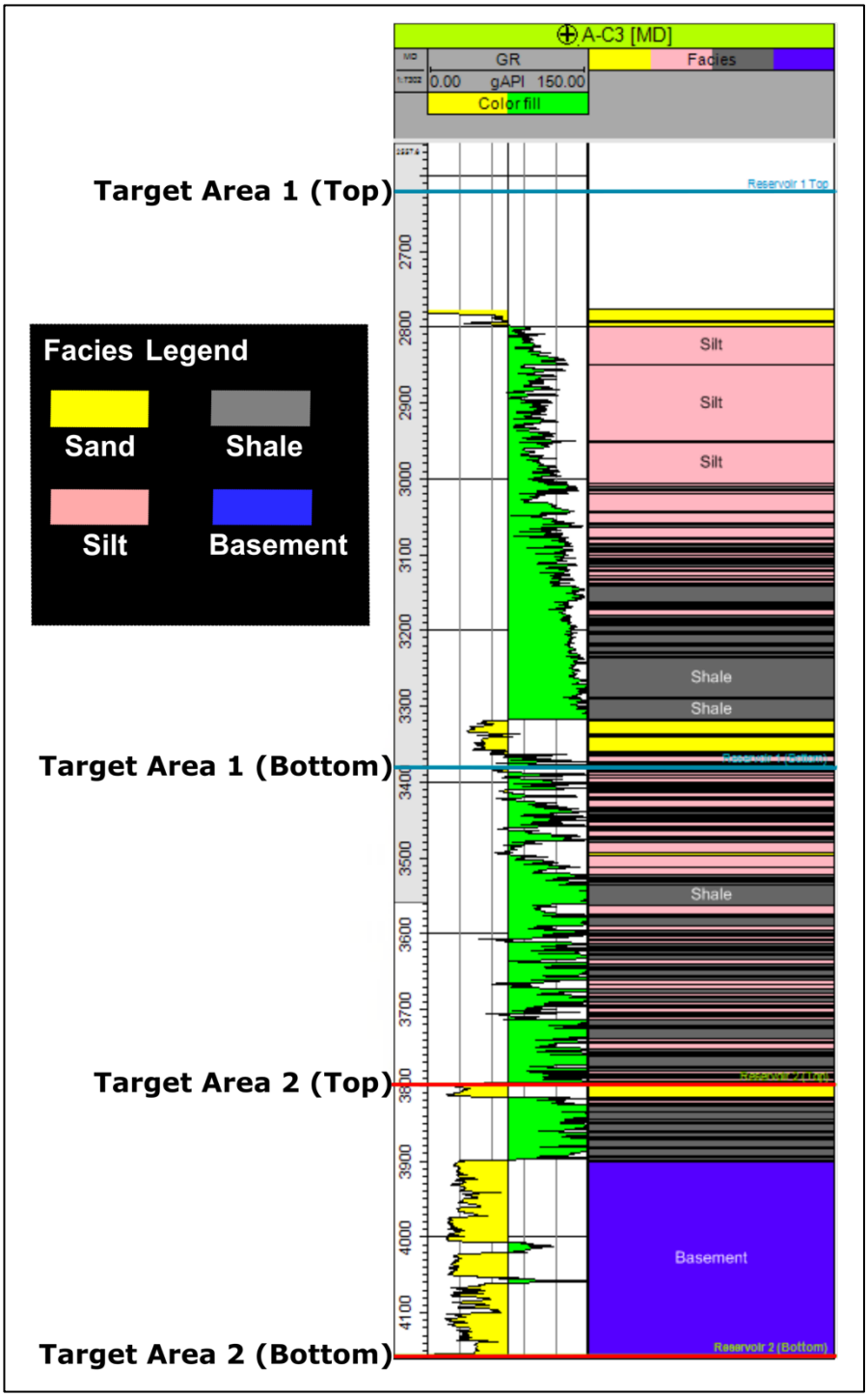

Figure 5.4. Displays the full well log of A-C3, which encompasses the potential target areas. The depth is in metres.

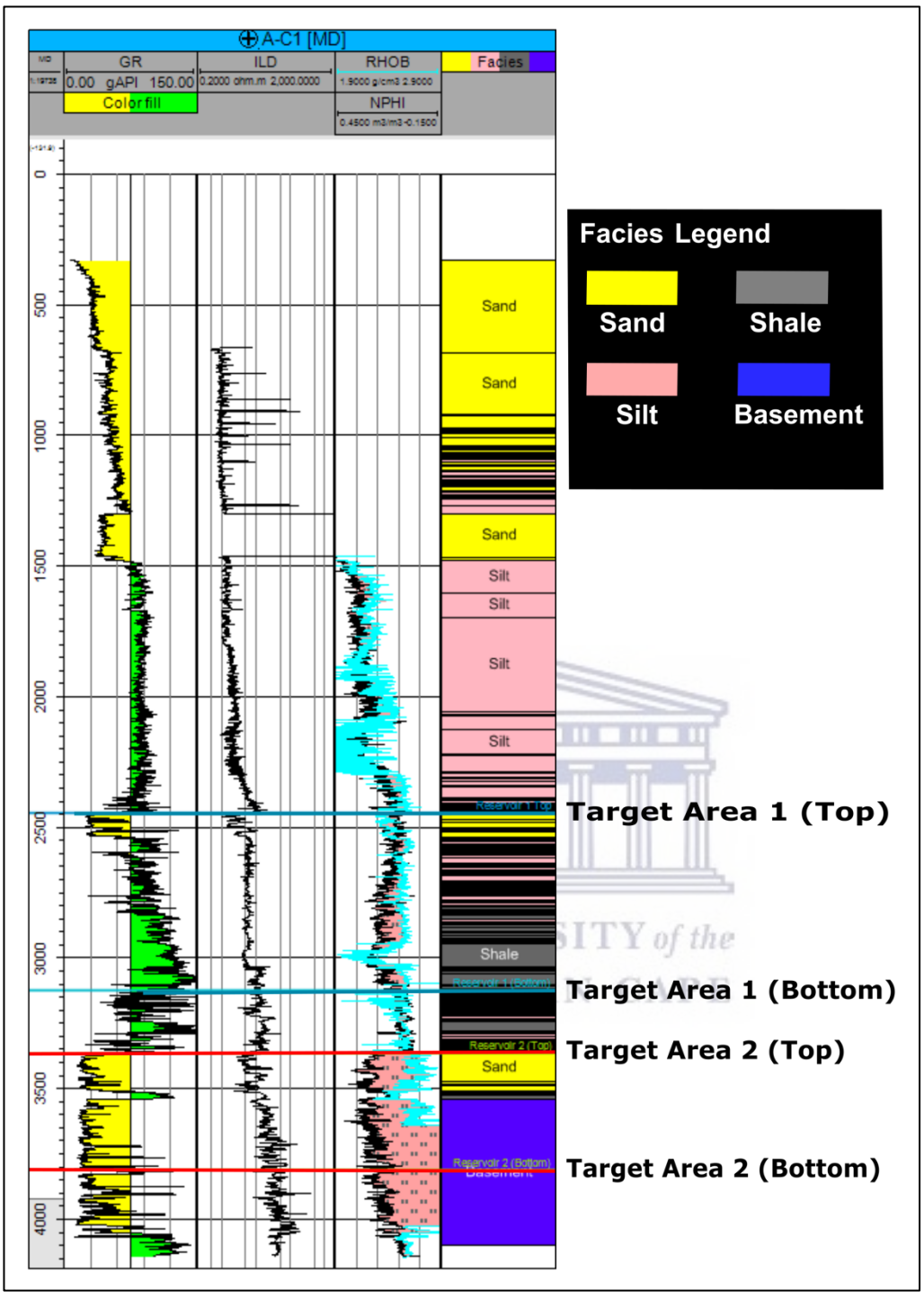

Figure 5.5. Logs for well A-C1 and the reservoirs have also been marked.

Referring to Figure 5.5, the resistivity log average in A-C1 is very low, with a value of 3,87 ohm.m. The resistivity throughout the well seems to be consistent. There are multiple sections that indicate gas pockets (hatched red section in the RHOB/NPHI tract), with the overall average for the density log is 2,5 g/cm^3 and 0,21 m^3/m^3 for the neutron porosity. The gas pockets are evident of the porosity log deflecting to the right, the density log deflecting to the left, as well as being far apart to one another. However,

in A-C1 from 3642 m to the bottom of Target Area 2 (3810 m), there is no density log and thus there is no way to critically say if and what hydrocarbons are present below 3642 m. The gas pockets are concentrated in the second target area compared to the first one. The gas pockets also coincide with the sand facies, indicating the possibility of a gas reservoir within the target areas.

Although the whole well of A-C2 ranges from 300 m to 3582 m. The log analysis displayed in Figure 5.6 only ranges from 2460 m to 3300 m. This is because A-C2 only has the first target area, thus the analysis is focused on that area with a buffer above and below the target area. Analysing the results of A-C2, the average ILD value is 14 ohm.m, even though the maximum is 162 ohm.m. The average density was lower than in A-C1, having a value of 1.4 g/cm^3. However, the average neutron porosity was higher, having a value of 0,78 m^3/m^3. Compared to A-C1, A-C2 has a few gas pockets, but they are very thin. However, the peaks that occur in the RHOB/NPHI tract coincide with changes in lithology seen on the gamma ray log.

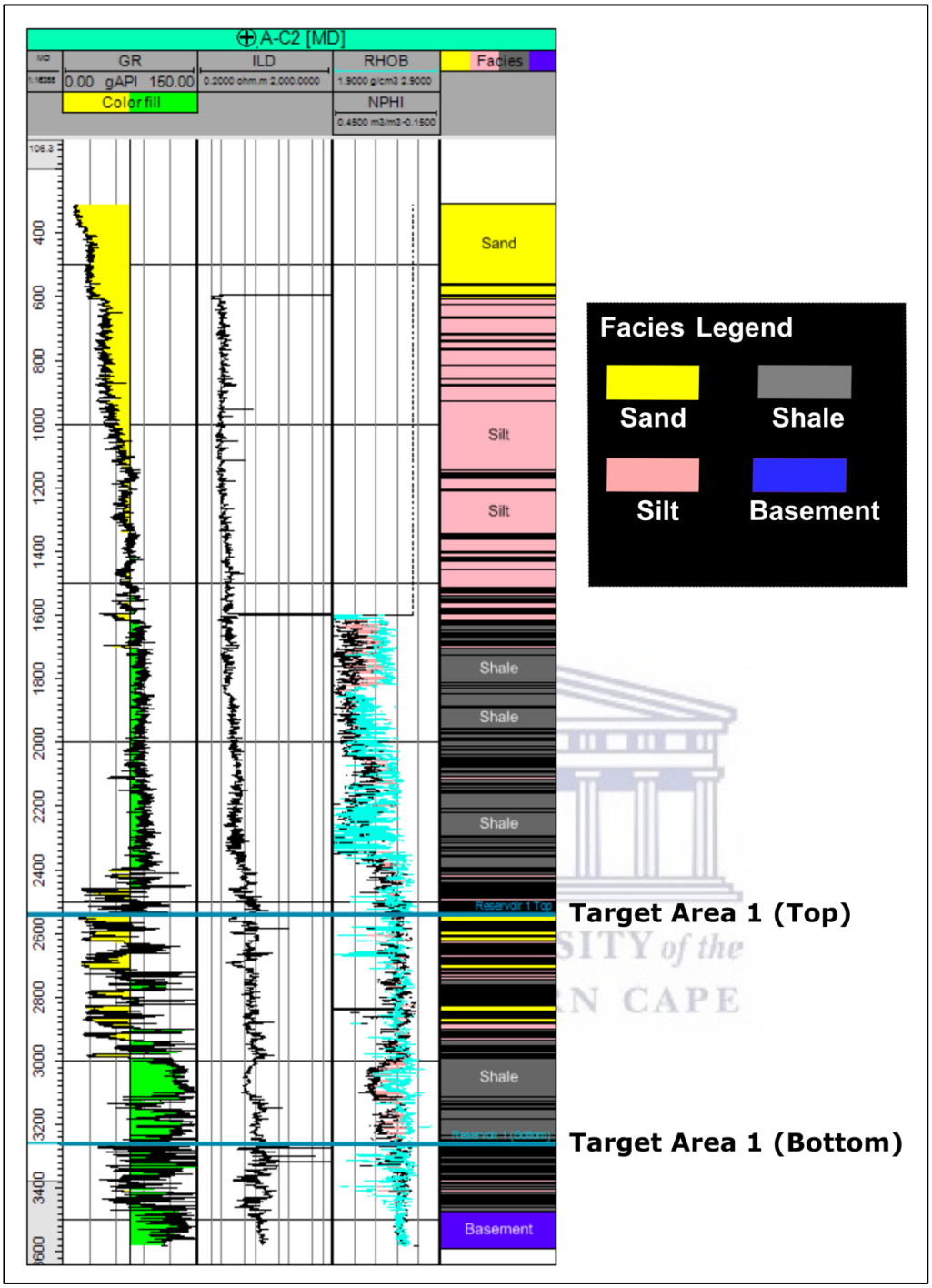

Figure 5.6. Logs for well A-C2 and the reservoirs have also been marked.

Similarly to A-C1, A-C3 has an average density and neutron porosity of 2.5 g/cm^3 and 0.2 m^3/m^3, respectively. The density log in A-C1 cuts off in the second target area, however in A-C3, it does not. Analysing Figure 5.7, similarly to A-C1, there seems to be a high concentration of gas in the second target area. Although there is small gas

pocket in the first target area, this present of gas was found in a similar position in the other two wells too.

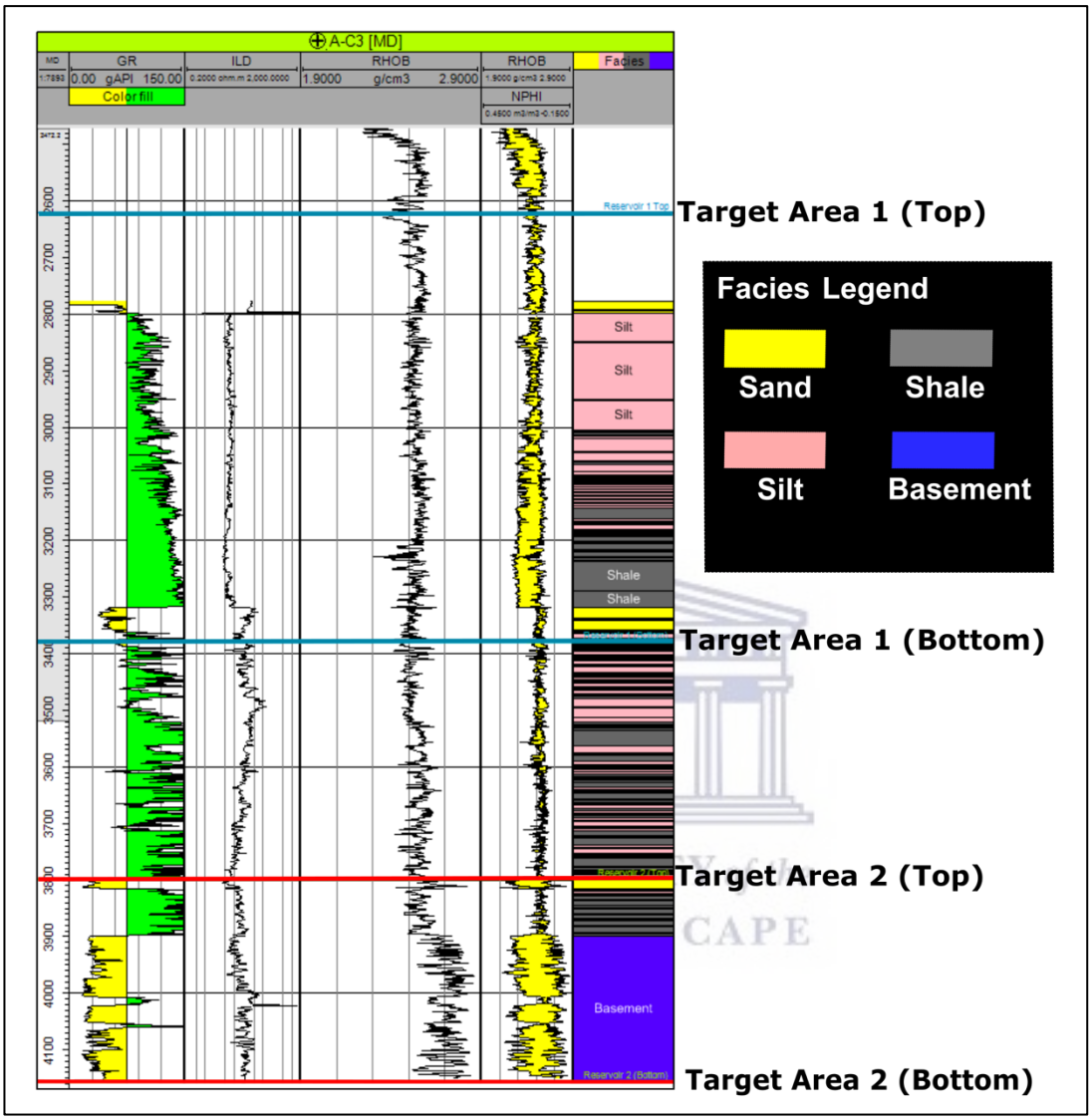

Figure 5.7. Logs for well A-C3 and the reservoirs have also been marked.

Figure 5.8 displays the effective porosity, permeability, water saturation and volume of shale for the whole of A-C1. These results are compared to the gamma ray tract to identify any correlations to the sand and shale areas in the well. The volume of shale (VSh) tract correlates perfectly to the gamma ray tract, with the peaks in the VSh tract matching with the dominant shale areas, shaded green in the gamma ray tract. The average volume of shale for the well is 0.3.

The average effective porosity is 0.2 m^3/m^3 out of a total of 1 m^3/m^3. Thus, indicating the porosity is very low in A-C1, which can be seen with the curve dominating the left

half of the tract. A similar patten can be seen in the permeability curve, which has an average of 60.5 mD out a total of 1000 mD. However, the permeability does increase as one moves down the well into the second target area, resulting in a higher permeability in the bottom half of the well, compared to the top half. Interestingly, the water saturation in the well is very high, with an average of 0.8.

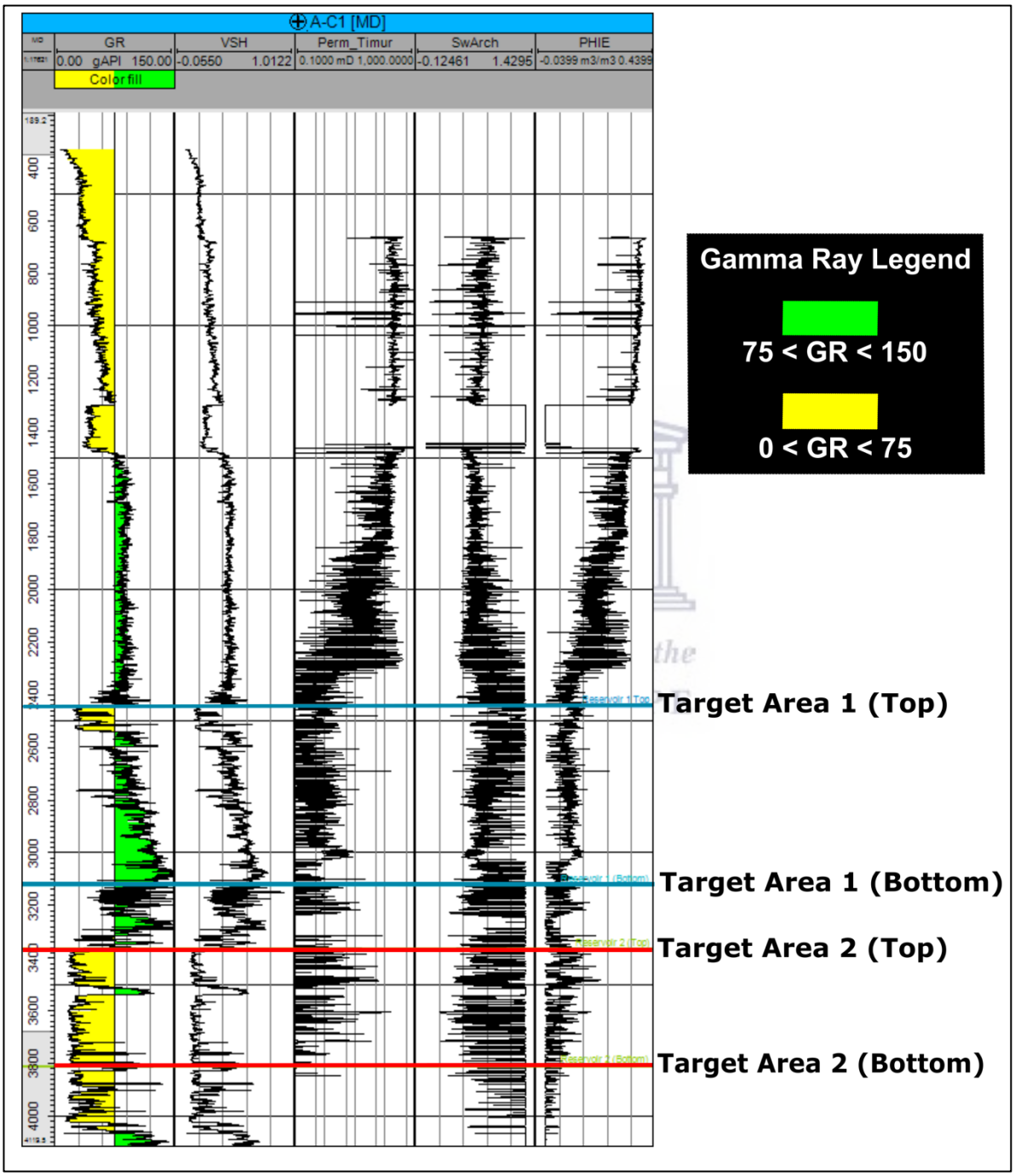

Figure 5.8. Log calculations for well A-C1. The depth is measured in metres.

A-C2 only has one target area, thus the length of the well displayed is slightly less than the other two wells. The results displayed in Figure 5.9, are different to A-C1. The volume of shale and water saturation is lower in A-C2, having an average of 0,02 and 0,7, respectively. This well contains more alternating sand and shale beds, thus creating a dirty sand signature. Although the volume of shale is lower, it is not a very clean sandy area. Also, there seems to be no consistency in the water saturation curve and the high and low peaks are in an almost random fashion.

The effective porosity increased by 10% to have a value of 0.3 m^3/m^3. Interestingly, the permeability increased to an average of 187 mD, which is the highest in all three wells. The high permeability peaks correlates very well to the sandy areas on the gamma ray log, indicating connectivity between the pore spaces despite the small sizes of the pores.

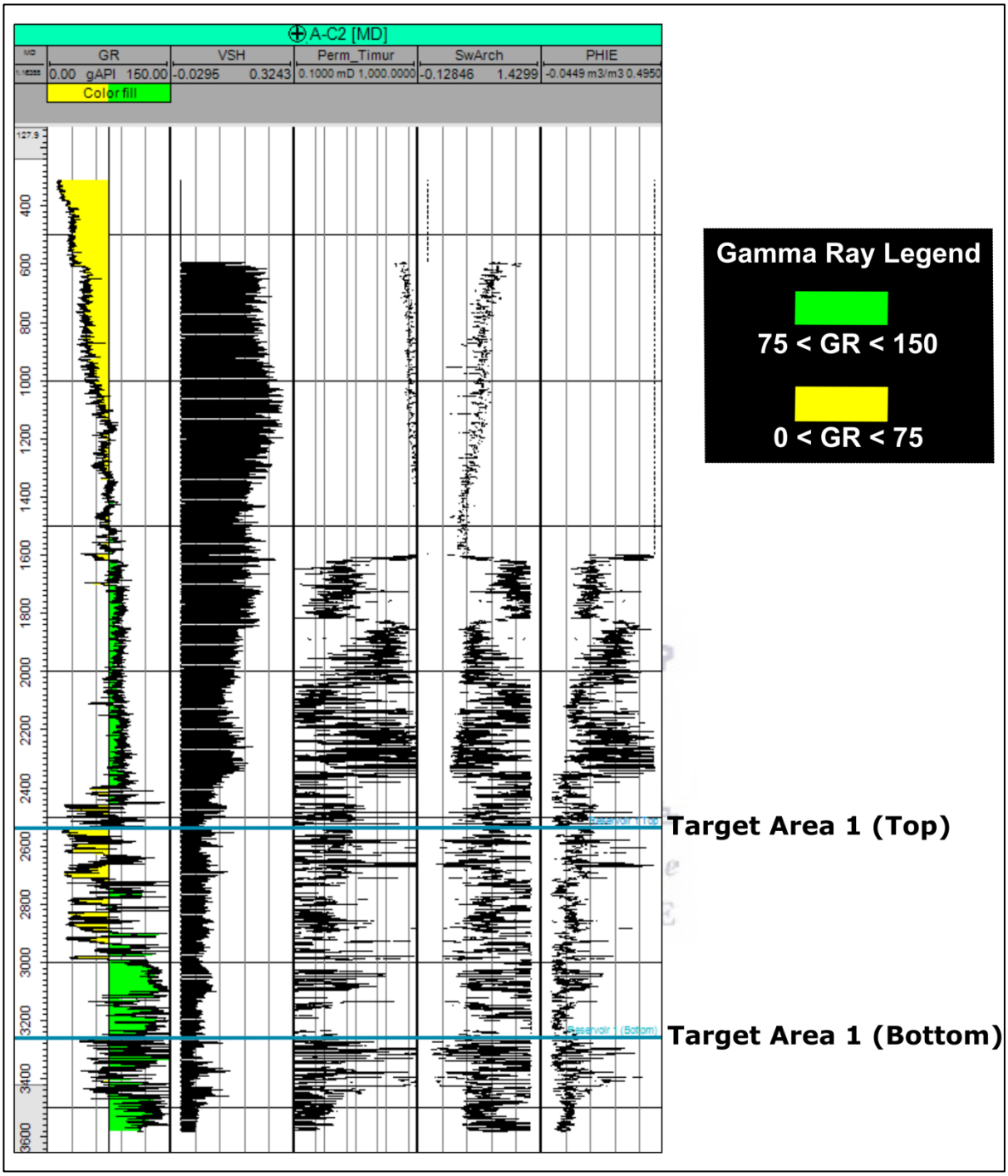

Figure 5.9. Log calculations for well A-C2. The depth is measured in metres.

Figure 5.10 displays the results for A-C3. Interestingly, the effective porosity starts off higher in the top half of the well, but then decreases considerably towards the end of the first target and at the start of the second area. It does increase towards the bottom of the well, but itis not by much, resulting in an average effective porosity is 0.1 m^3/m^3.

The average permeability is greater than in A-C1, but only has an average of 17 mD, which is very poor. These initial results indicate that A-C3 has very low porosity and these pores are not connected either. The other observation is that the permeability and porosity curves are very similar. They peak at exactly the same areas, except that the permeability peaks are bigger. However, unlike in the other two wells, the water saturation is considerably lower, having a value of 0.4. The water saturation curve does not seem to change drastically, although it increases, when both the porosity and permeability decreases toward the bottom of the first target area. The water saturation then decreases moving from the top of Target Area 2 to the bottom, contrary to the permeability and porosity which increases. An interesting anomaly is the sand area at the bottom of the first target area, where both the porosity and permeability actually decreased, instead of increasing as it did higher up in the well. Although the VSh curve only starts from the bottom of the first target area, it does show the same trend as the gamma ray curve.

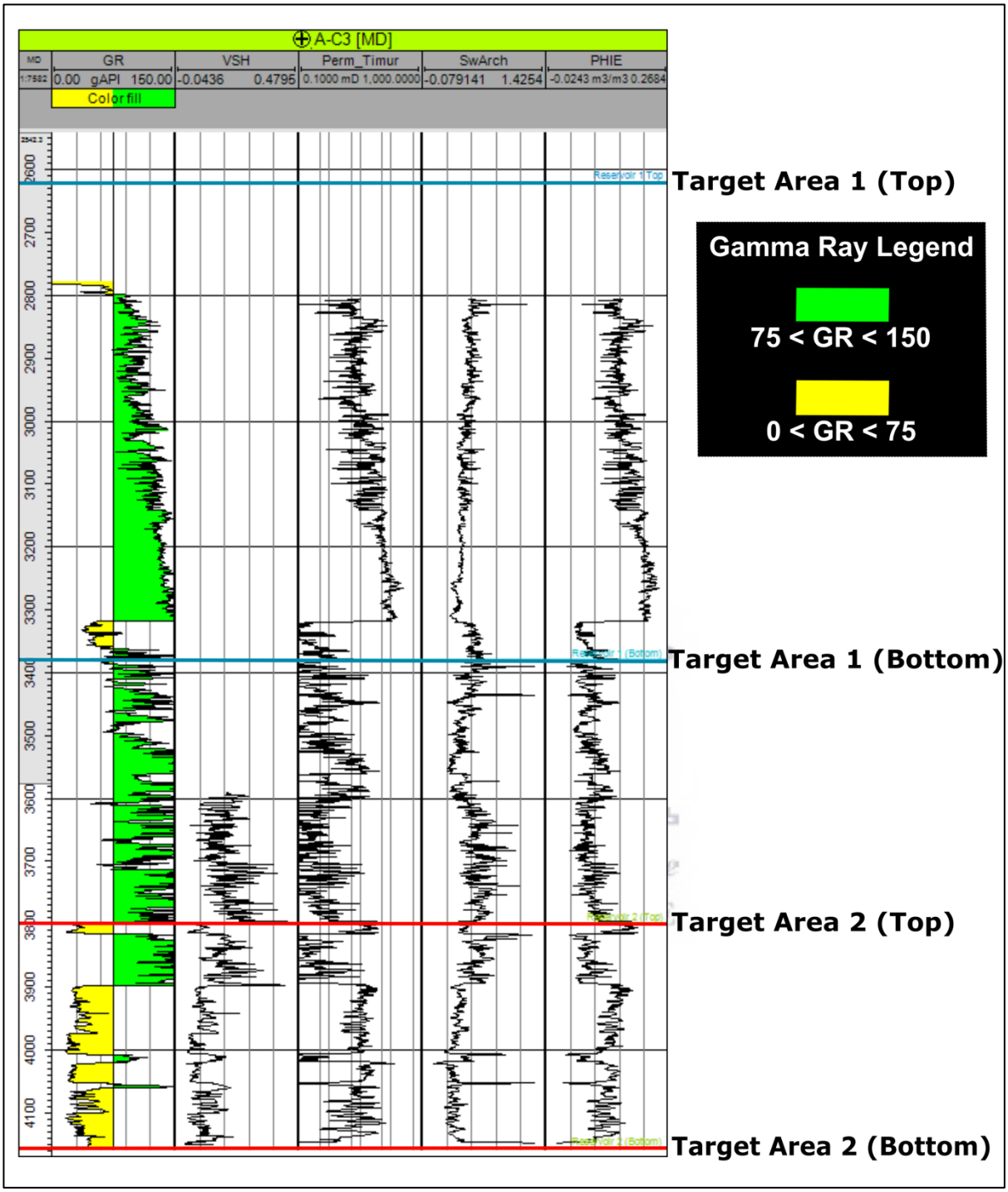

Figure 5.10. Log calculations for well A-C3. The depth is measured in metres.

5.3 Modelling

A total of six models were produced for each targeted area, which were mapped for the whole study area. These six models made up the properties that formed the reservoir characterisation. The five properties were:

- Facies (Figure 6.1 and Figure 6.2)
- Volume of shale (Figure 6.3 and Figure 6.4)
- Effective porosity (Figure 6.5 and Figure 6.6)
- Permeability (Timur method) (Figure 6.7 and Figure 6.8)
- Water saturation (Archie Method) (Figure 6.9 and Figure 6.10)
- Recoverable gas (Figure 6.11 and Figure 6.12)

The petroleum models correlate the petrophysical and the geophysical data, to create a greater picture of the combined data. For this reason, it will be discussed in the next chapter – **Chapter 6 Discussion**.

6. CHAPTER 6: Discussion

The results presented in Chapter 5: **Results** show two target areas, which both have a prospective reservoir. Both of these targeted areas were identified in wells A-C1 and A-C3. However, only *Targeted Area 1* was identified in A-C2. Thus, the second targeted area was mapped for the greater study area applying the data from A-C1 and A-C3.

6.1 Facies model

Targeted Area 1 (Figure 6.1) contains 18,5 % sand, 37.2% silt and 44.4% shale. The sand is concentrated in the uppermost region of the area around A-C1 and A-C2. However, around A-C1, it occurs at depths of 2445 m to 2544 m, compared to A-C2 which is a lot thicker (2534 m to 2990 m). This sand area is compartmentalised and alternates with thin layers of shale.

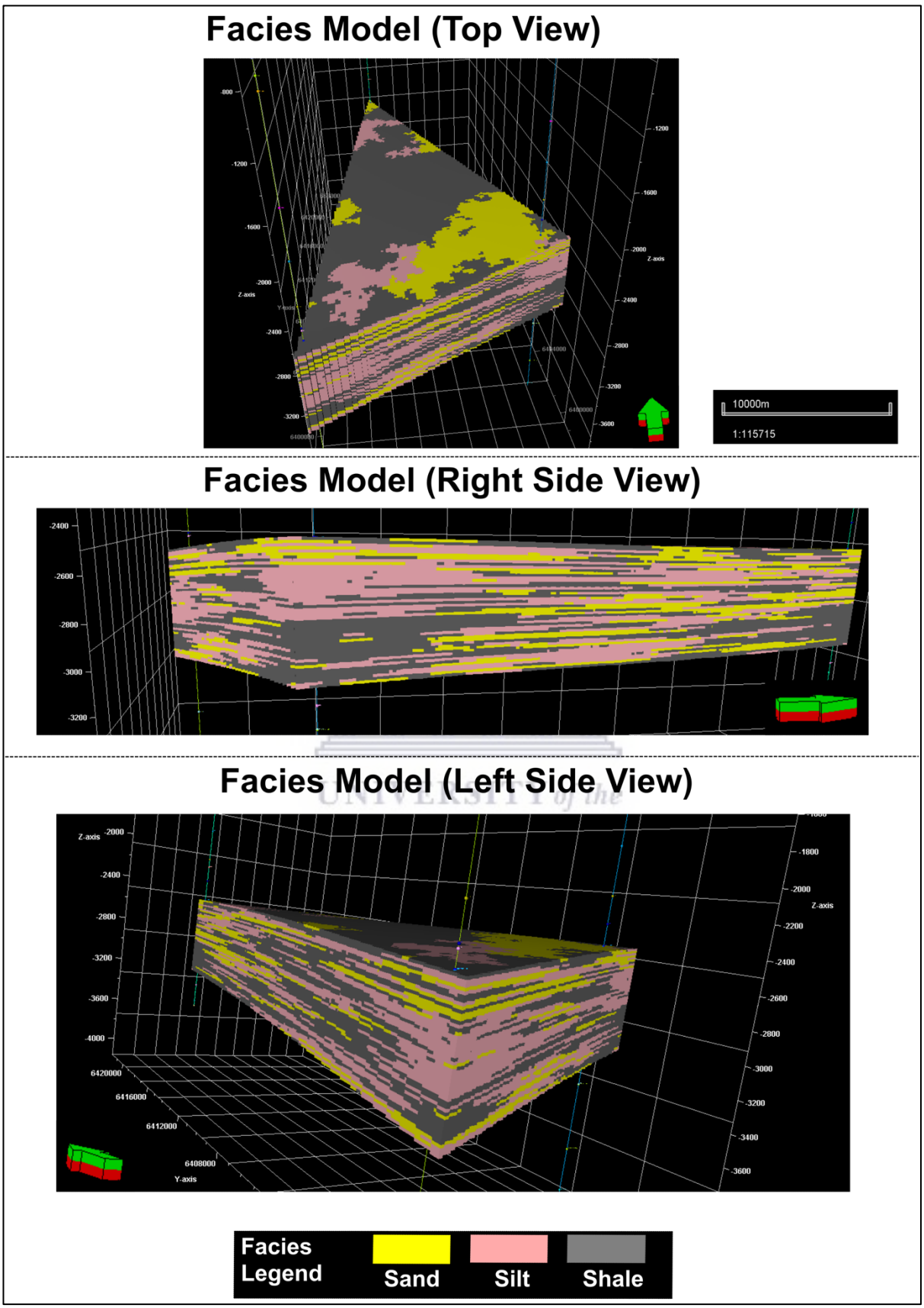

Figure 6.1. Displays the Facies model for Target Area 1 from three different sides. Scale bar is the same for all figures.

In A-C3, there is only a thin section of sand, the sand portion has a thickness of 43 m. Silt makes up a considerable amount and is located in the middle of the targeted area and is the dominant facies in A-C3. However, the concentration of shale in the targeted area is the majority. This is partly because of the dominance of shale in A-C2. At the top of the targeted area, the shale is located in the centre of the study area. However, at the bottom of the targeted area, the shale is concentred near A-C2 and becomes sand in the middle of the area and then silty near A-C3 and silty-shale near A-C1.

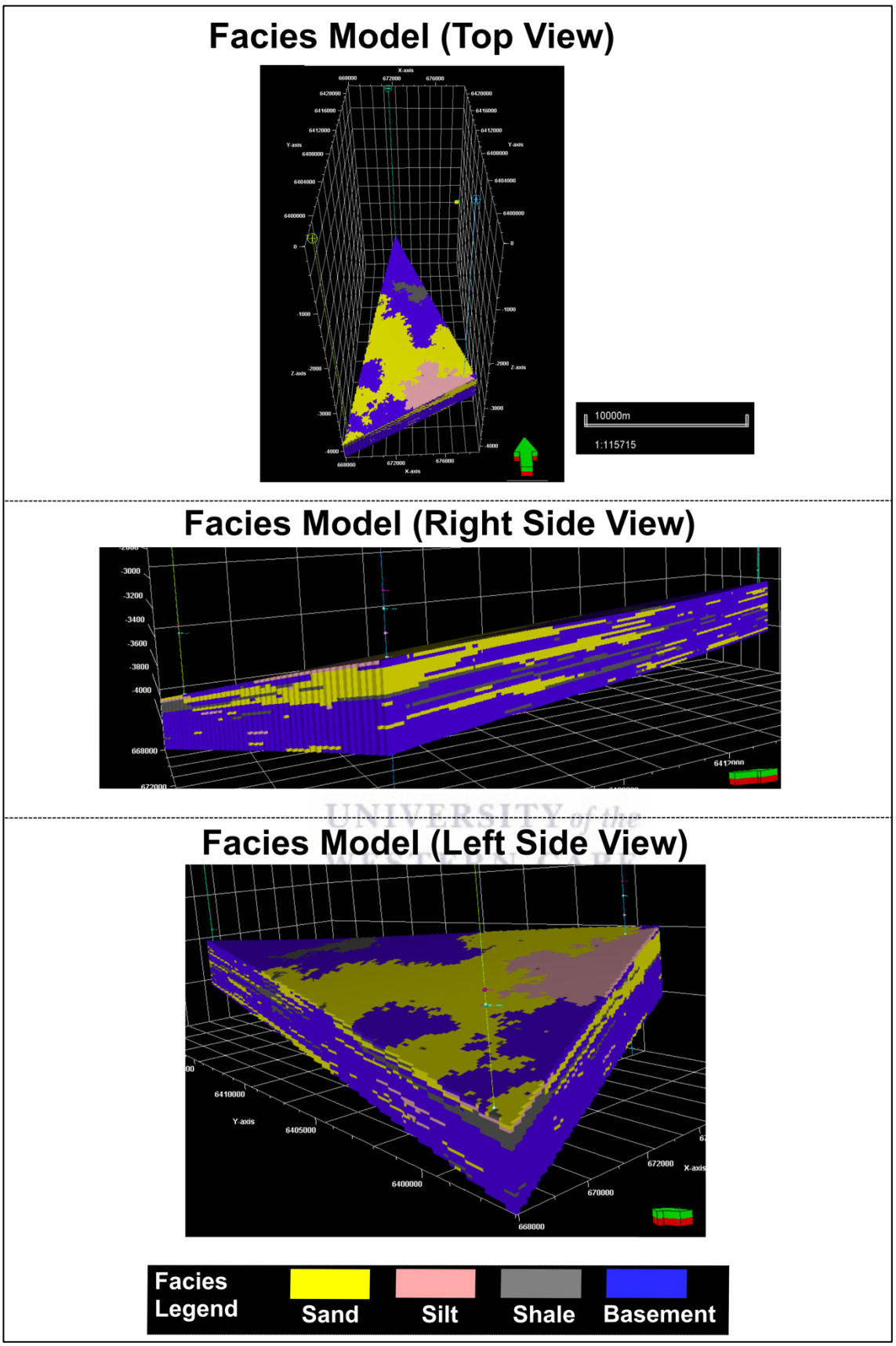

Figure 6.2. Displays the Facies model for Target Area 2 from three different sides. Scale bar is the same for all figures.

Comparing the facies model from *Target Area 1* (Figure 6.1) to *Target Area 2 (*Figure 6.2*)* , the first observation is the addition of another facies. From the well top 6At1 to the bottom of the target area is basement. With the improvement of technology, oil and gas exploration is now extending to the basement too. In the second targeted area, the basement facies makes up 68,1% of the area. This compares to 21,7% of sand, 1,4 % of silt and 8,9% of shale.

The sand facies is concentrated near A-C1 and has a relative thickness in the study area of around 145 m. However, this sand area thins out as one moves seaward towards A-C3 and northward towards A-C2. The top of the target area is concentred with silt and changes to sand towards the centre of the area towards A-C2. However, around A-C2, the basement is predominant. The basement facies begins from around 3539 m in A-C1, compared to 3900 m in A-C3. Similarly to Target Area 1, a sand area in the second targeted area above the basement facies is compartmentalised.

6.2 Volume of shale

The next property that was modelled was the volume of shale (VSh). This property is similar to the facies model in the sense it displays a difference in facies. However, this model displays the areas where there is a high shale concentration and a low shale concentration. A high shale concentration would indicate a possible cap rock area, whereas a low shale concentration would indicate a potential reservoir, and thus would be similar to where the sand pockets are in the facies model.

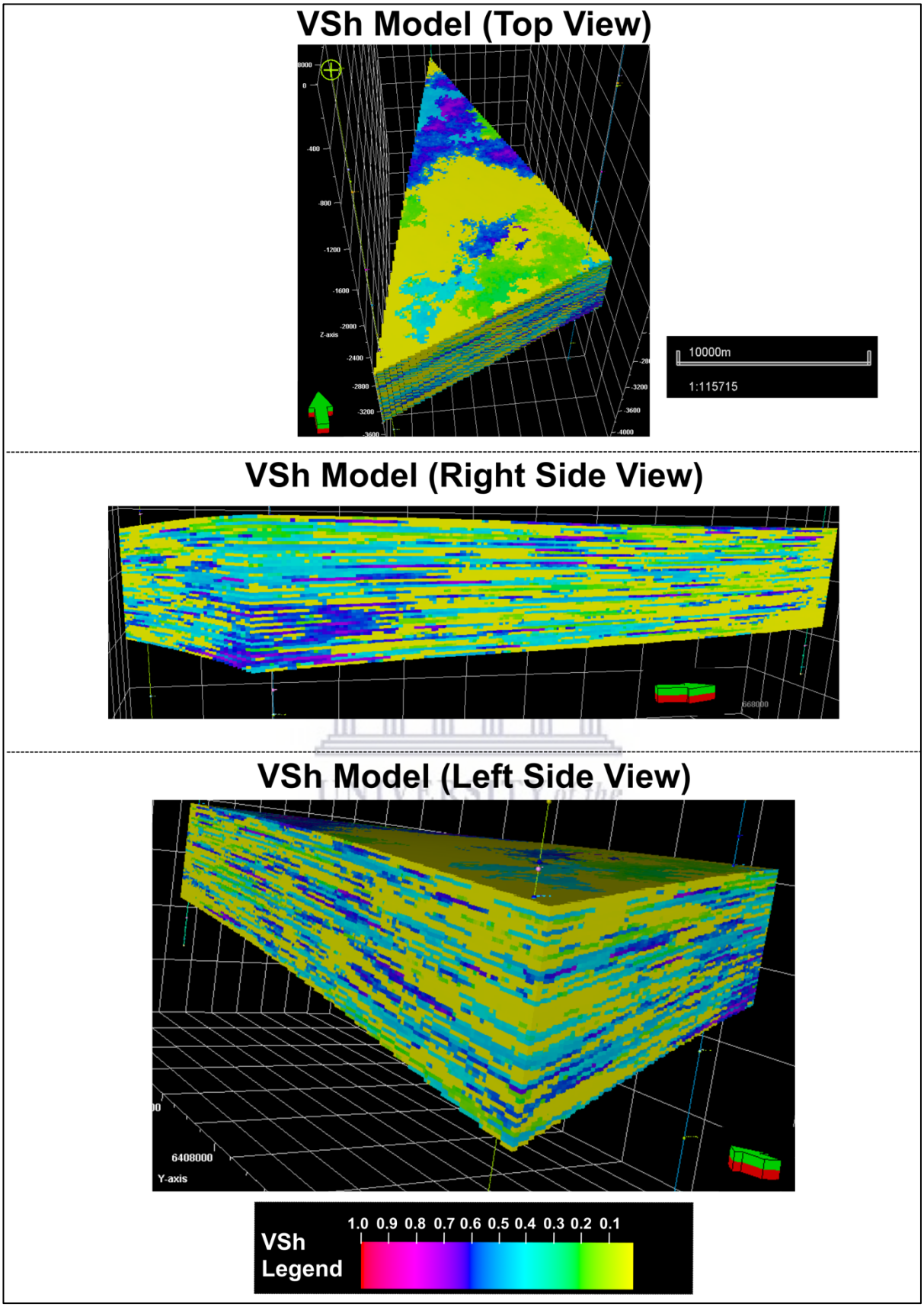

Figure 6.3. Displays the Volume of Shale (VSh) model for Target Area 1 from three different sides. Scale bar is the same for all figures.

In Target Area 1 (Figure 6.3), the high concentration of shale at the top of the target area is near well A-C2, compared to the area near A-C1 and A-C3 that has a low shale content. However, this changes as you move deeper in the target area, the shale concentration increases at the bottom of both A-C1 and A-C3, indicating a possible cap rock at the bottom of the target area.

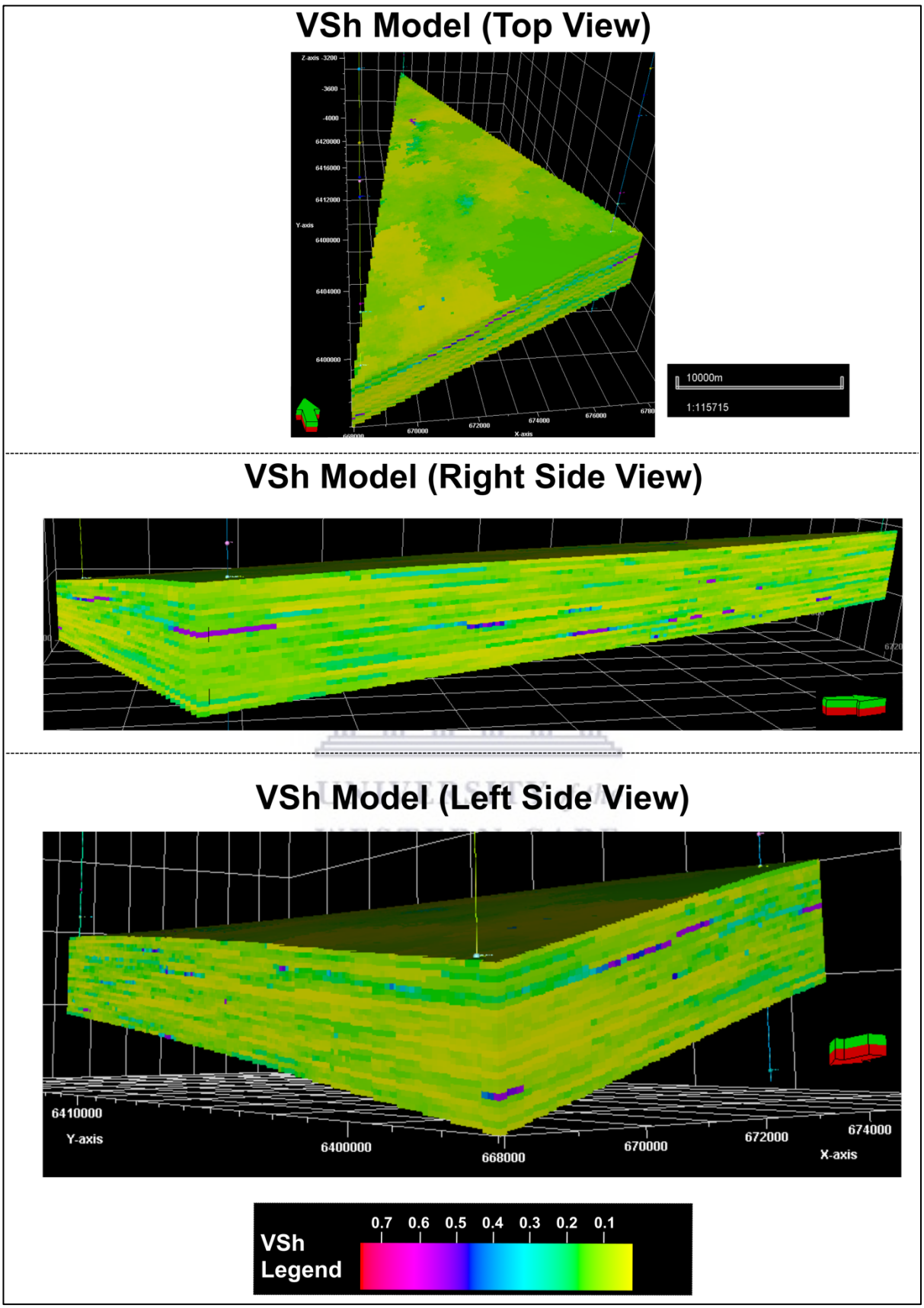

Figure 6.4. Displays the Volume of Shale (VSh) model for Target Area 1 from three different sides. Scale bar is the same for all figures.

In Target Area 2 (Figure 6.4), the concentration of shale is actually very low through the whole study area. The only region of a high shale volume is at 3500 m near A-C1, and 3900 m near A-C3. The areas of low shale content correlate to the basement facies in the second target area.

6.3 Effective porosity model

Porosity is an important characteristic in a reservoir characterisation, because the fluids are stored in the pore spaces within the rock. However, these fluids could either be oil, gas or water. High porosity areas (where the porosity value is closer to 1) could indicate a potential hydrocarbon reservoir. The porosity is very low for majority of Target Area 1 (Figure 6.5), ranging from 0,0001 to 0,45 m^3/m^3. Particularly the sand identified area near A-C1, which has very low porosity values, ranging from 0,09 to 0,15 m^3/m^3. Thus, it may not be a potential reservoir. There is an increase in porosity from around a depth of 3000 m to 3300 m around A-C3, ranging from 0,17 to 0,21 m^3/m^3. At this depth there are scattered pockets of higher porosity throughout the study area. This area near A-C3, however, corresponds to the silt and shaly areas in the facies model. There is also a relatively higher porosity at the top of the Target Area near A-C2. However, for the average porosity for Target Area 1 is 0,23 m^3/m^3, indicating poor porosity in the area.

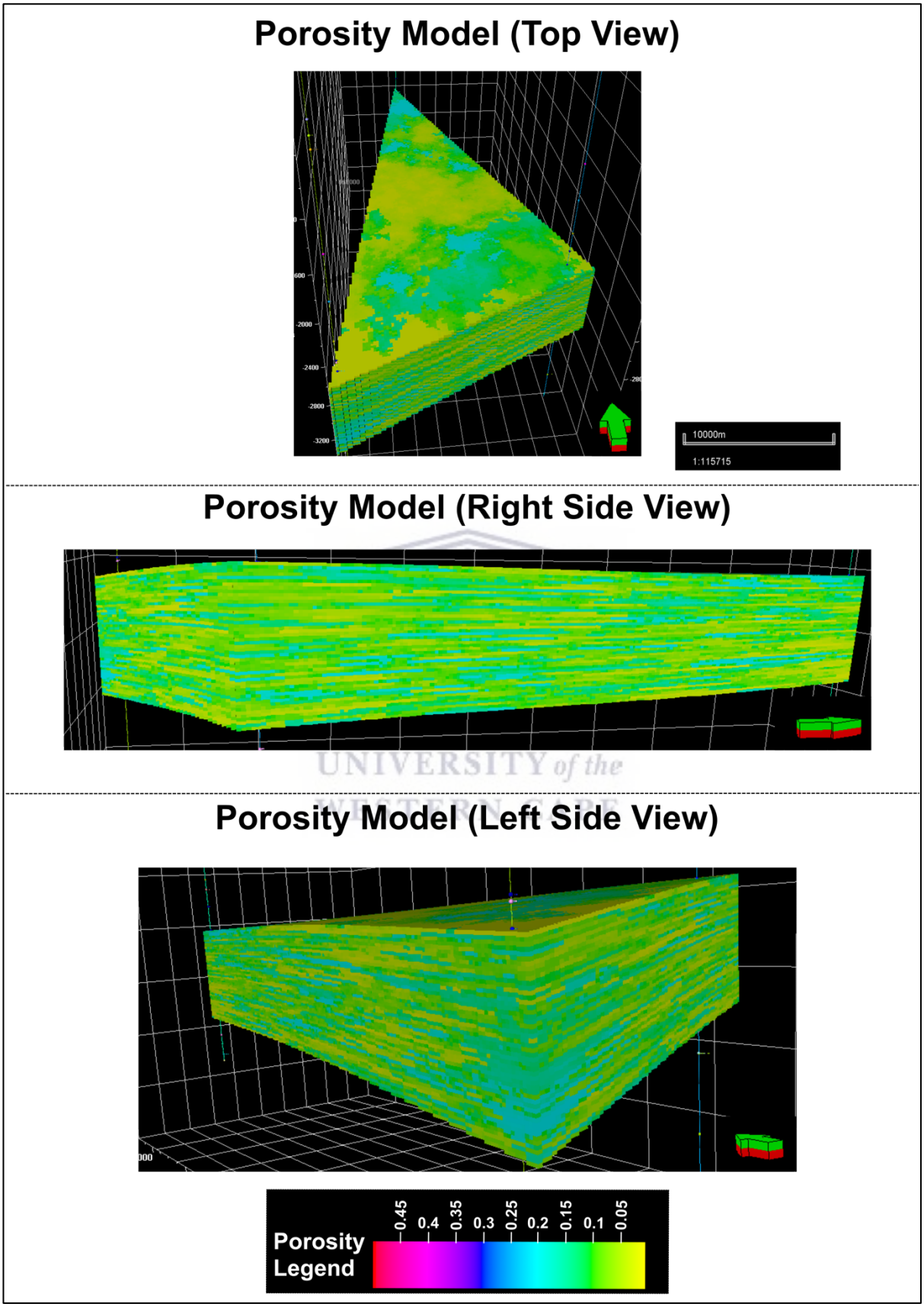

Figure 6.5. Displays the Effective Porosity model for Target Area 1 from three different sides. Scale bar is the same for all figures.

Target Area 2 (Figure 6.5) has even lower porosity values to Target Area 1. The porosity hardly changes throughout the target area, with a maximum porosity value of 0,61. However, these low porosity values correlate to the facies of the area, which is predominantly basement.

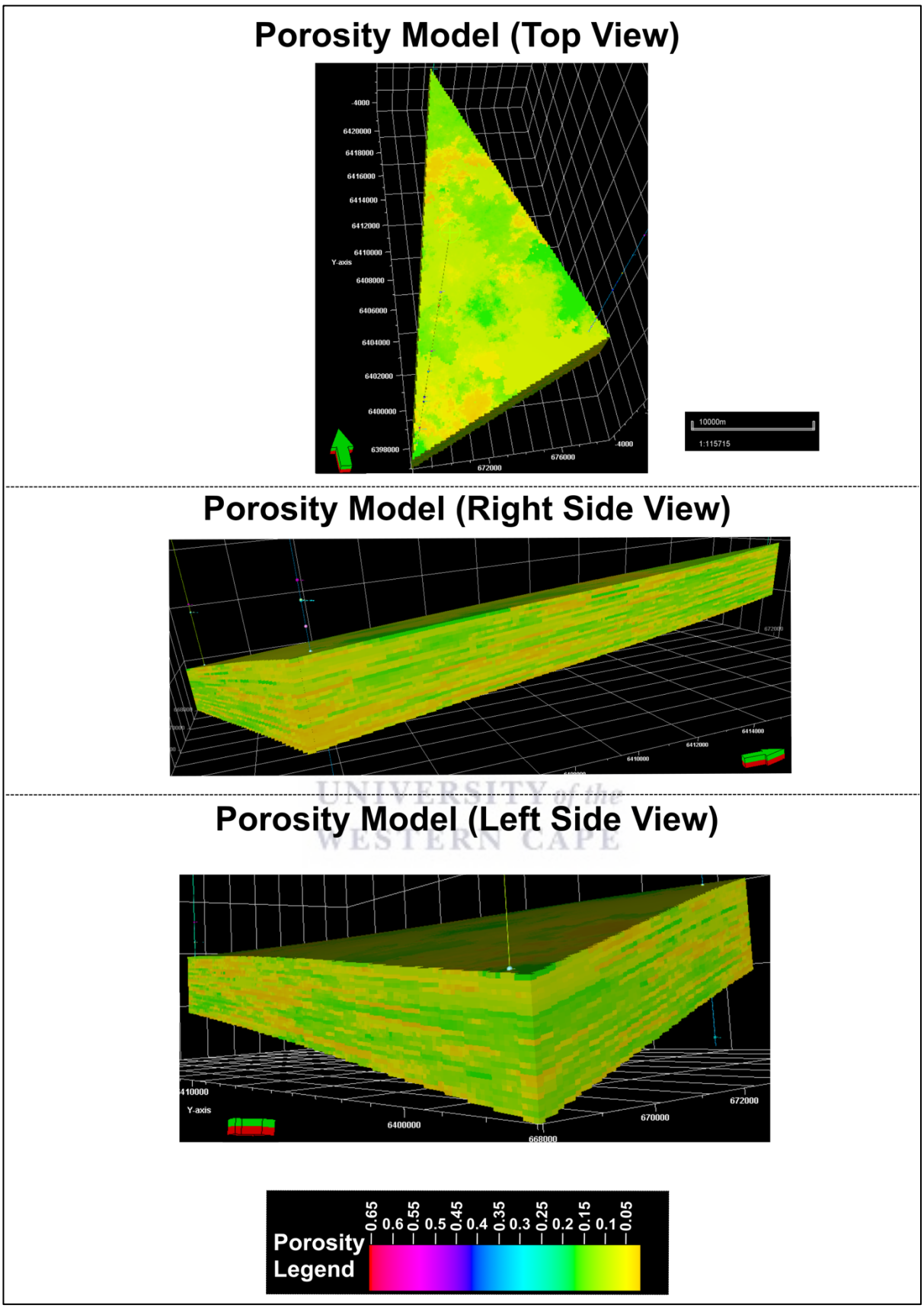

Figure 6.6. Displays the Effective Porosity model for Target Area 2 from three different sides. The green arrow indicates the direction of North. The range is from 0.0 to 0.65.

6.4 Permeability model

Permeability relates to the measurement of how easily a fluid can pass through a porous medium. It also looks at the connectivity of the pores in an area. If there is low permeability, but high porosity, it implies that those porous areas are connected. The relationship of permeability and porosity looks at describing the reservoir rock capacity with regards to the fluids ability to move.

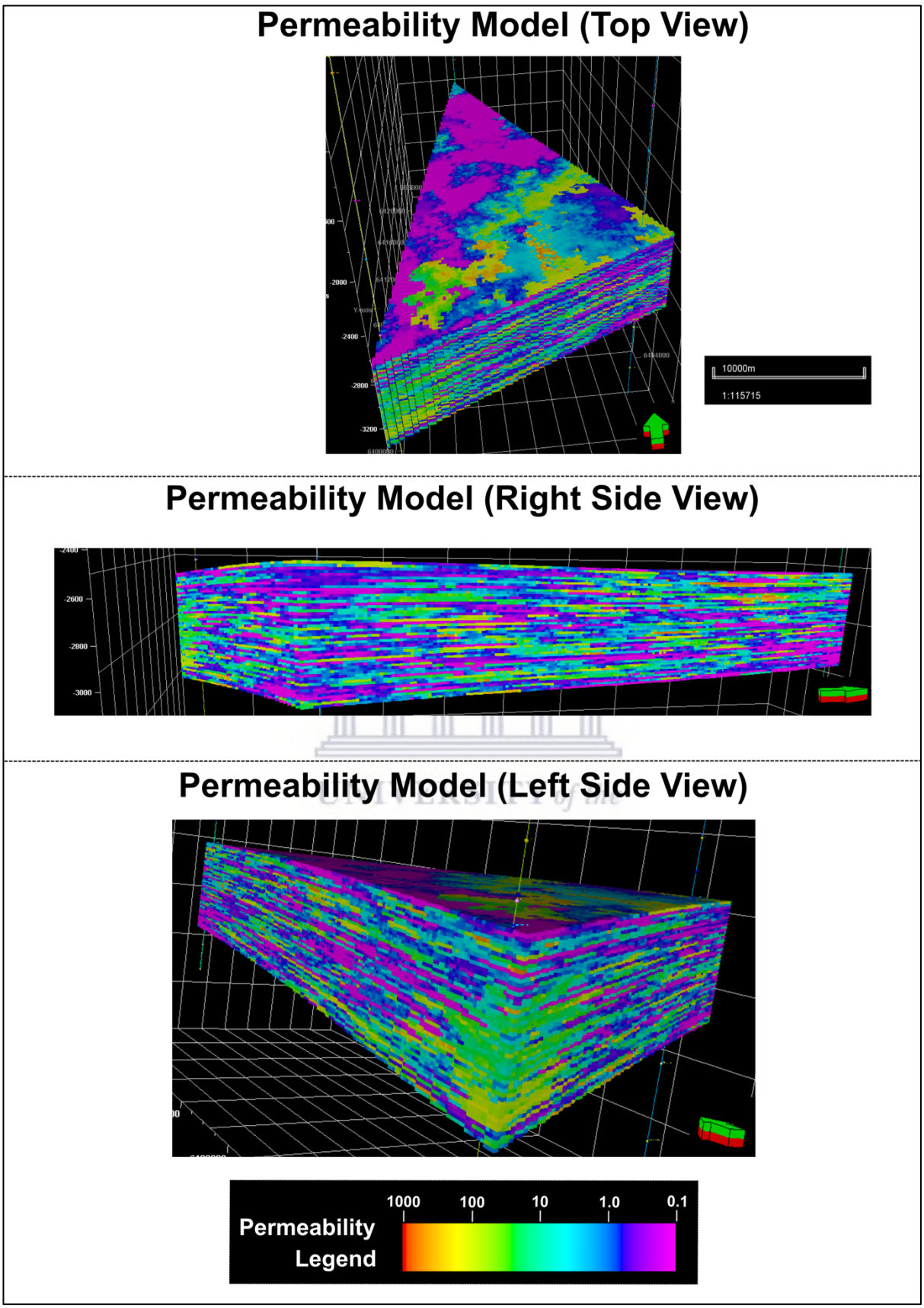

Figure 6.7. Displays the Permeability model for Target Area 1 from three different sides. Scale bar is the same for all figures.

The relationship of permeability and porosity in Target Area 1 (Figure 6.7) is very similar. At the top of the target area, the region around A-C1 (a radius of 7000 m) initially the permeability is low, ranging from 0,8 to 4,2 mD, but towards both A-C3 and A-C2, the permeability drops to very poor permeability, ranging from 0,1 to 0,8 mD. Interestingly, this pattern is also seen at the base of Target Area 1. Just like the porosity, the permeability increases from around a depth of 2800 m all the way to the bottom of the target area, ranging from 5,6 to 138. This signature does not extend laterally through the Target Area. Although, there are one or two regions where there is an increase in permeability, this does not continue, and thus majority of the permeability is poor to fair. There are very low permeability values around A-C1, except for a slight increase around a depth of 2800 m, which goes from 0,6 to 3,3 mD.

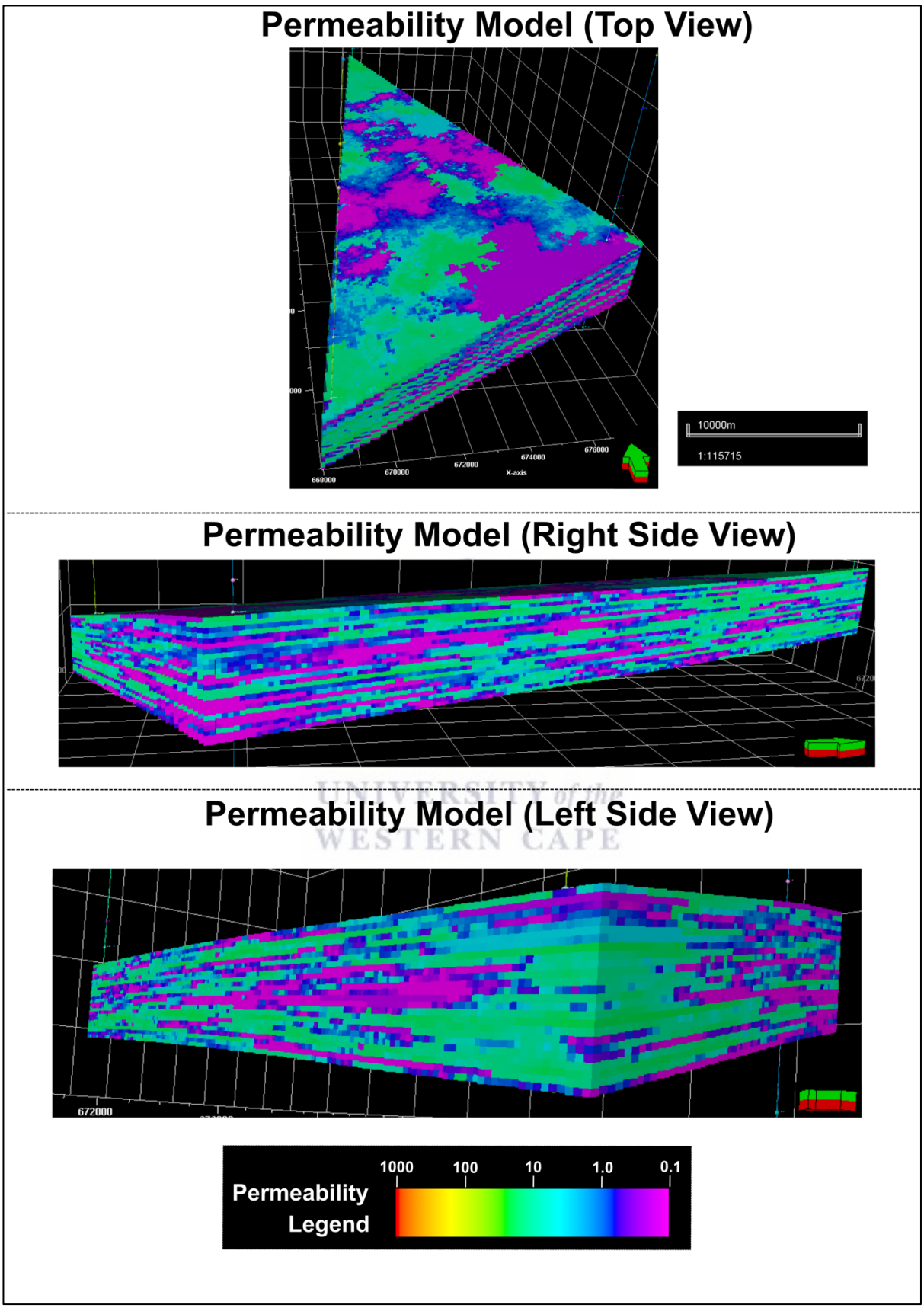

Figure 6.8. Displays the Permeability model for Target Area 2 from three different sides. Scale bar is the same for all figures.

Compared to Target Area 2 (Figure 6.8), the permeability is overall poor to fair, generally less than 25 mD. The maximum permeability is considerably lower in the Target Area 1. However, the basement area around A-C2 and A-C3 has the highest permeability in the Target Area 2. This indicates that the basement has good connectivity. Although, the area around A-C1 has very poor permeability from a depth of 3200 m to 3800 m, with an average value of 0,93 mD. There is a small pocket where the permeability does increase slightly to an average of 16,2 mD, at a depth of 4000 m. This area correlates to the change in facies from shale to basement.

6.5 Water saturation

Water saturation is an important characteristic of a reservoir characterisation, because it provides an estimation of the percentage of the pore space occupied by water compared to oil or gas. After identifying where the porosity is high, it is important to determine what they are filled with.

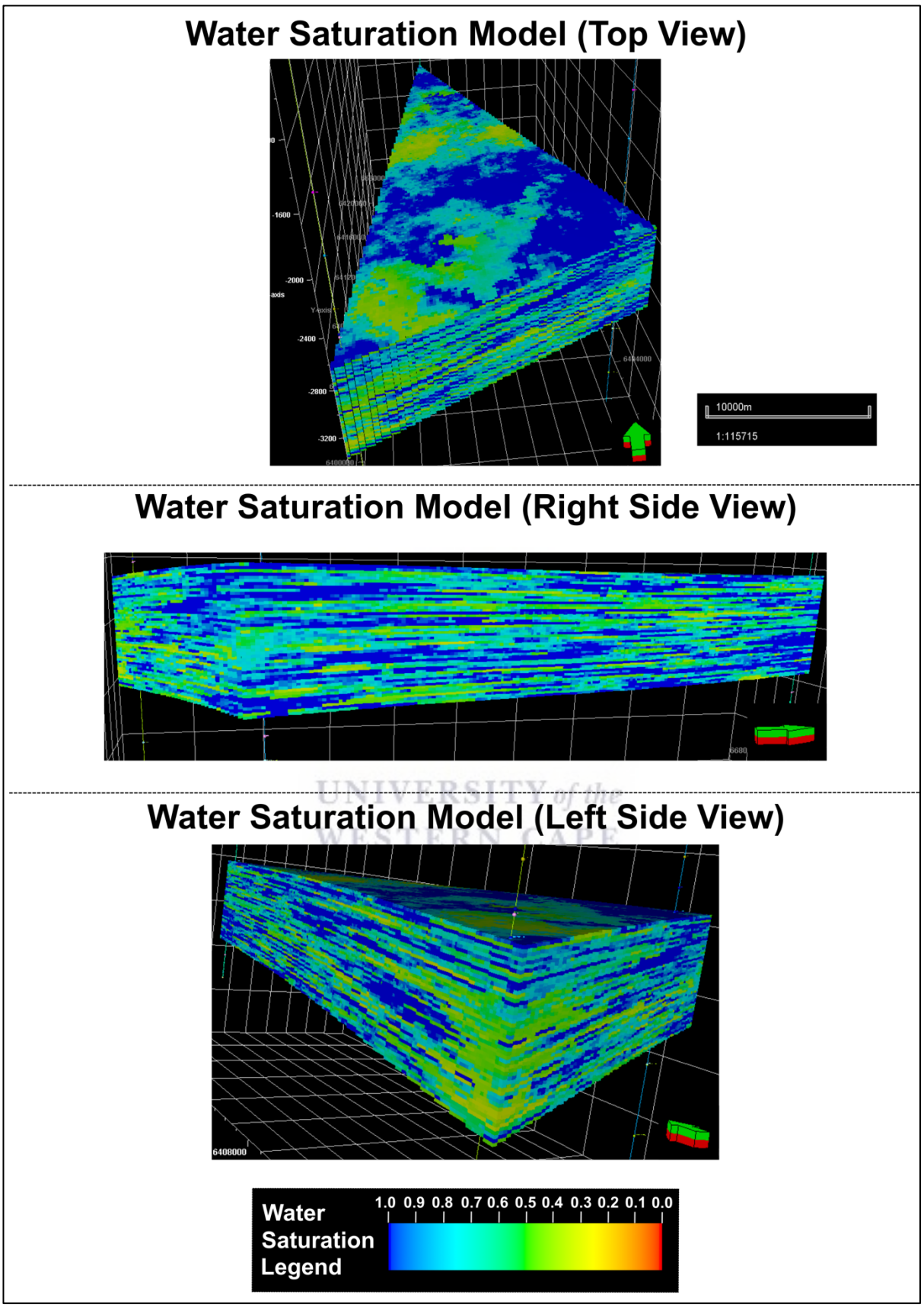

Figure 6.9. Displays the Water Saturation model for Target Area 1 from three different sides. Scale bar is the same for all figures.

Referring to Target Area 1 (Figure 6.9), majority of the area has high water saturation, with an average value of 0,65. This high percentage of water saturation is predominantly concentrated in the silty shale and shaly areas of the area. However, there are sandy areas, which have a high volume of water. This is near sandy pockets north of A-C1. Around A-C1, the water saturation is volume is the highest with an average value of 0,8. In fact, the whole study area is water saturated and the lowest volume is 0,3.

In terms of hydrocarbon accumulation, the concern with the high volume of water saturation in the sand areas is that, it shows signs of a potential reservoir. However, because the water saturation is so high, it could mean that the sand portion is full of water and not hydrocarbons.

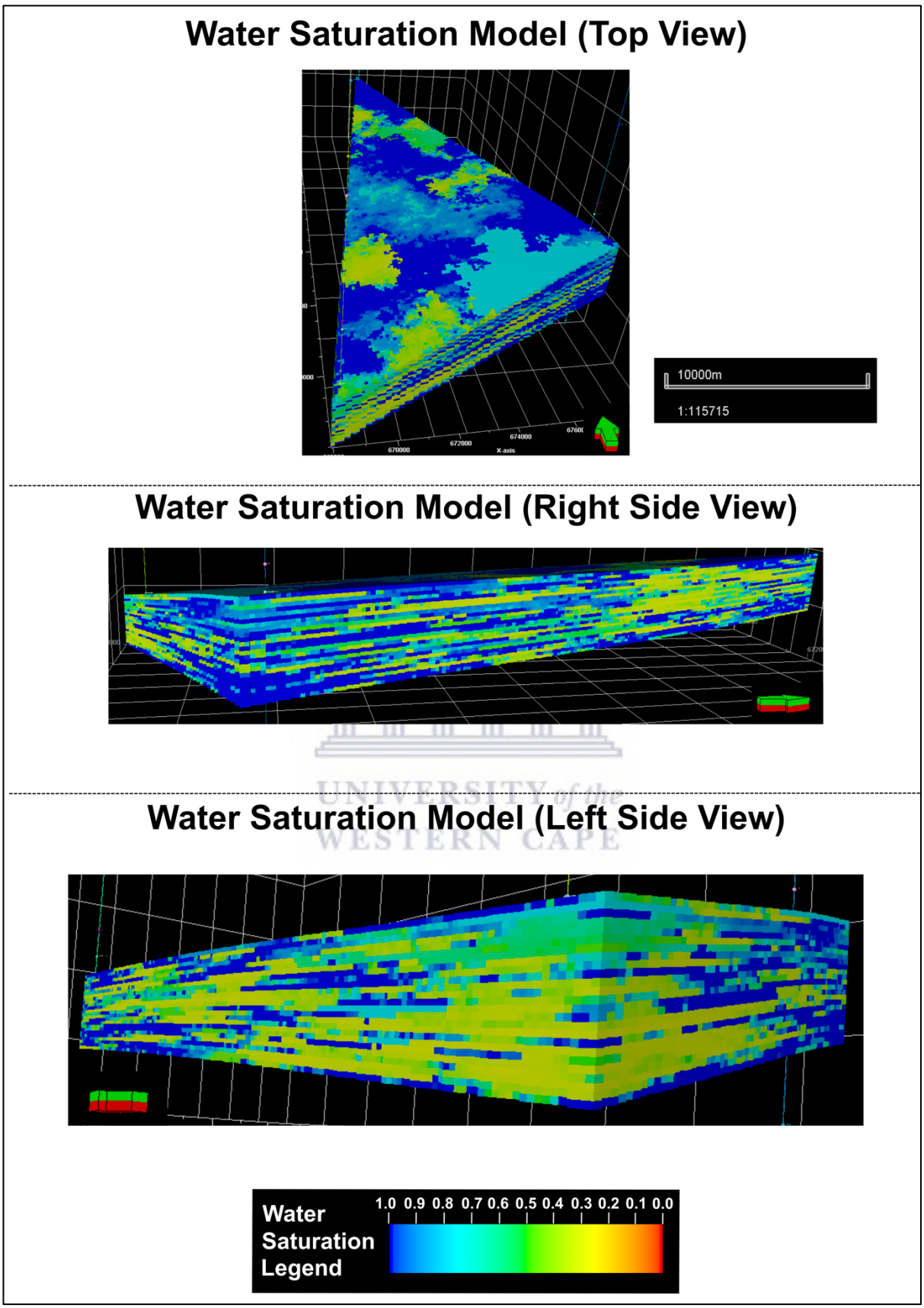

Figure 6.10. Displays the Water Saturation model for Target Area 2 from three different sides. Scale bar is the same for all figures.

Comparing this to Target Area 2 (Figure 6.10), there is a similar trend of a high volume of water 7around A-C1. However, in majority of the basement areas, the water saturation is relatively low compared to the rest of the Target Area 2 and Target Area 1. Interestingly, the silt area located at the top bounding layer between A-C1 and A-C3 has exactly the same outline for water saturation, as it does in the facies model and permeability model. The low volume of water saturation is concentrated around the bottom of A-C3 as well as in an area around 7 km south of A-C2. This area is predominantly made up of shale and basement, correlating to the low porosity, resulting in the pores that are present to be most likely filled with water.

Initially, the gamma ray log was used to identify two target areas. The analyses of five properties in the first target area revealed that the zones of interest that display the potential of a petroleum reservoir are from 2400 m to 2600 m and then at 2900 m to 3200 m, throughout the entire study area. Using the density and neutron logs, it was determined that the hydrocarbon present was gas and not oil throughout Target Area 1. At the depth of 2400 m to 2600 m, the porosity and permeability are high at both A-C1 and A-C2, however these properties thin out towards A-C3. This thinning out was observed on the gamma ray log in the first target area. Although, the shale content is high at the top of this zone and may possibly cap rock, the water saturation was high in this zone, especially around A-C1.

The second zone (2900 m to 3200 m), displayed the results of a more promising potential reservoir. The porosity and permeability were considerably higher in this region, particularly around A-C3. The porosity and permeability became, but remained fair, away from A-C3 landward and northward. The volume of shale varied across this zone, but it definitely provided a cap rock at the base of the zone at a depth of 3200 m. Lastly, the water saturation was considerably lower around A-C3 and A-C1. However, the water saturation increases near A-C2. The bulk of the high water saturation is concentrated around A-C1. However, at a depth of 4000 m in A-C3 and a depth of 3700 m in A-C2 the water saturation is very low. Those pores could presently be filled with water.

6.6 Recoverable gas model

Finally, the net to gross was calculated in this in Target Area 1 (combining the potential reservoirs), using the formula;

$\frac{Net}{Gross} \leq 1$ (Egbele *et al*., 2005)

Where:
Net is the total thickness of the zone areas (potential reservoirs)
Gross is the total thickness of the target area

The net to gross value for Target Area 1, was $\frac{500}{800} = 0{,}625$. Therefore 0,625 of the first target area had the potential to be a reservoir.

The second target area, which was mapped from a depth of 3363 m to 4150 m is the entire potential area. This is because it initially starts with a sand facies at the top of A-C1, it then thins out towards A-C3 and A-C2. There is a layer of shale separating the sand above and the basement below, but this shale layer is very thin and could be the reason for the reservoir to be compartmentalised. The porosity values do fluctuate within the basement, but it is not very different to the porosity observed in the sand layer at the top of the Target Area. Using the density and neutron porosity logs, it was identified that gas is present in this area too. Although, there is a section in A-C1 that loses the density curve, thus it cannot be said if the gas continues in this area. The gas is identified around A-C3 in a similar depth. The shale layer separating the basement and sand is very thin, potentially resulting in gas travelling up from the basement to the sand. The net to gross in Target Area 2 is 0,84, because in both A-C1 and A-C3, there is a shale package towards the top of the Target Area.

After calculating the net to gross in each target area, the volumetrics of each target area was calculated. It was determined that both the bulk volume and the recoverable gas was greater in Target Area 2, compared to Target Area 1, with values of 151 923 sm^3 and 95 057 sm^3, respectively. The gas to water contact was identified in Target Area 1 at a depth of about 3500 m around A-C1 and A-C3, and about 2900 m around

A-C2. This contact can be seen by the yellow shaded area at the bottom of the model in Figure 6.11 and the blue shaded area in Figure 6.12. Figure 6.11 shows that the recoverable gas in Target Area 1 is around 90 000 sm^3. After performing the volumetric calculation, it was determined that the bulk volume in Target Area 1 is 152 091 sm^3, yet the recoverable gas is only 95 057 sm^3. Figure 6.12 displays that the recoverable gas in Target Area 2 is around 140 000 sm^3. After performing the volumetric calculation, it was determined that although the bulk volume in Target Area 2 is 180 860 sm^3, the recoverable gas is 151 923 sm^3.

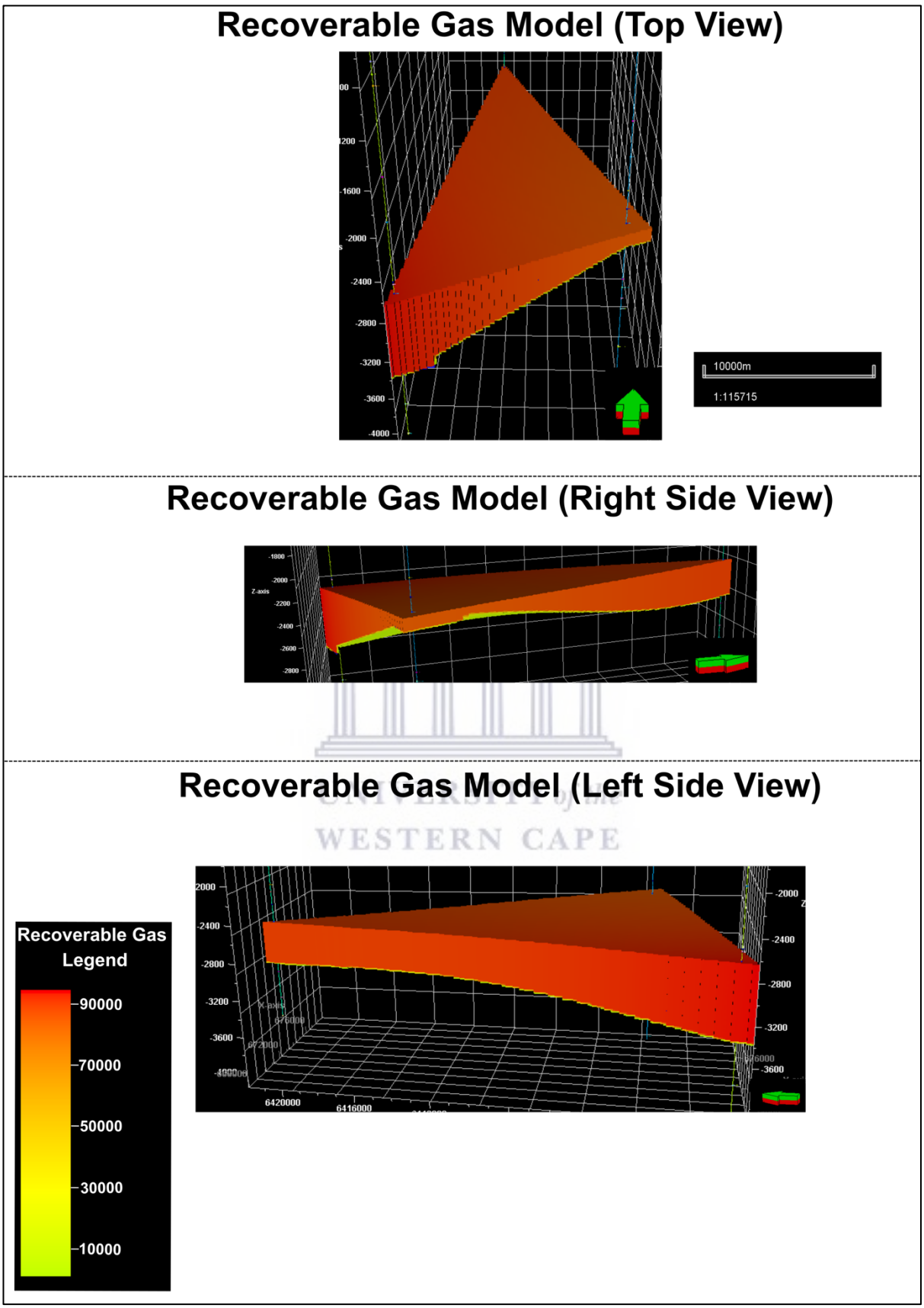

Figure 6.11. Displays the Recoverable Gas model for Target Area 1 from three different sides. Scale bar is the same for all figures.

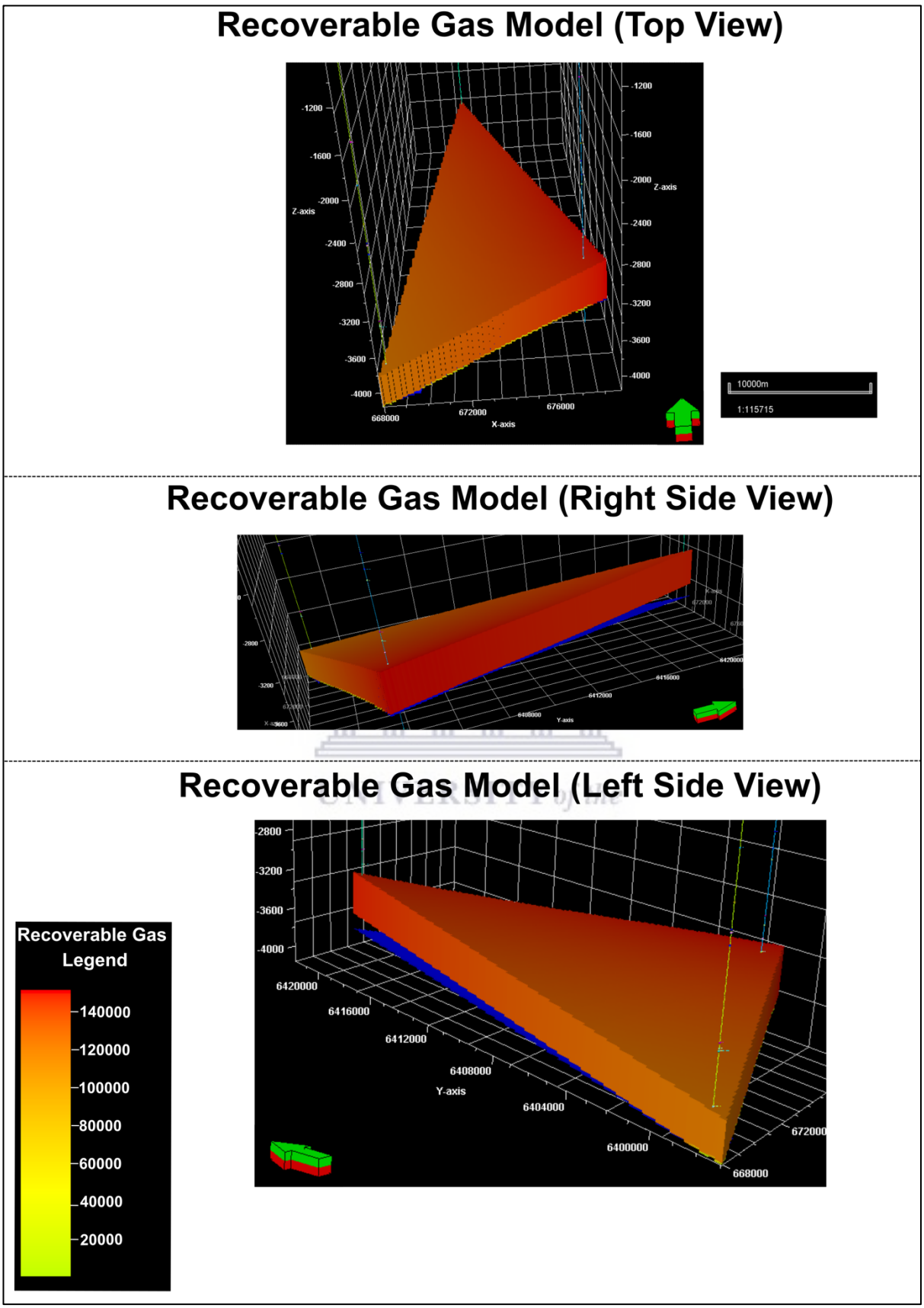

Figure 6.12. Displays the Recoverable Gas model for Target Area 2 from three different sides. The blue shaded area indicate the water-gas contact. Scale bar is the same for all figures.

The data from both models (Figure 6.11 and Figure 6.12) is summarised in Table 6.2. The table indicates that although there is a decent volume of space available in both wells, the recoverable gas is still poor. However, the Ibhubesi Gas field located in the northern area of the Orange Basin was calculated to contain 540 billion cubic feet of gas.

Table 6.2 Summarises volumetrics in the target areas

	Target Area 1	**Target Area 2**
Net to Gross Ratio	0,625	0,84
Bulk Volume (sm^3)	152 091	180 860
Recoverable Gas (sm^3)	95 057	151 923

6.7 Interactions among all models

Table 6.3 and Table 6.4 summarises the reservoir characteristics in each target area for an easier comparison.

Table 6.3 Summarises the characteristics for Target Area 1

Target Area 1	VSh	Porosity	Permeability (mD)	Water Saturation
Min	0,0074	0,0001	0,001	0,3
Max	0,7064	0,45	571,25	1
Average	0,3569	0,22505	285,6255	0,65
Percentage (%)	36	23		65

Table 6.4 Summarises the characteristics for Target Area 2

Target Area 2	VSh	Porosity	Permeability (mD)	Water Saturation
Min	0,0368	0,0001	0	0,2779
Max	0,5465	0,2213	20	1
Average	0,29165	0,1107	10	0,63895
Percentage (%)	29	11		64

The main concern with both areas being potential reservoirs, could be that the permeability is very low. Although, there are pores available, there does not seem to be much connectivity. Poor permeability and porosity are two characteristics of tight gas reservoirs (Bahadori, 2014). Tight gas reservoirs contain natural dry gas and the poor permeability and porosity which could be as a result of the geology in the area or a high clay content.

The findings based on the A-C1 and A-C3 well reports showed that there was a high clay content in the matrix of the sandstone. The high clay content was proposed to be a result of the depositional environment. These environments were determined to be deposited as barrier bars, or as shoreline deposits lateral to a delta (SOEKOR, 1991, Larsen, 1994). This is because of the presence of argillaceous materials, indicating a high supply of terrestrial material. From the well reports it was hypothesised that wells located farther seaward may have a better petroleum potential, because the input of terrestrial material would reduce. The analysis of the data in A-C3 revealed that the potential for a reservoir would be in this well.

The second Target Area in A-C3 has the presence of gas and low water saturation too. According to the well report, it was concluded that A-C3, although more seaward, does not have a great improvement in hydrocarbons compared to the other two wells, even though a source rock was intersected when drilling the exploratory well (Larsen, 1994). A potential reason for this could be that the interpretative software has improved largely since the study was carried out, thus resulting in modern interpretative techniques identifying data that was not previously identified.

In order for tight reservoirs to be economical, hydraulic fracturing needs to take place to increase the permeability. Consequently, it would increase the hydraulic conductivity in the reservoir and cause an increase in the flow of the gas in the reservoir. The poor permeability in Target Area 2 could lead to the reservoir being compartmentalised. Compartmentalisation occurs when there are a number of separations in an area, resulting in individual fluid compartments occurring in areas where there are accumulation of hydrocarbons (Jolley *et al*., 2010). In Target Area 2, according to Jolley *et al*. (2010), the compartmentalisation could be a result of *dynamic seals*, which occurs when there are low to very low permeability rates, resulting in the flow of hydrocarbons to be minuscule. Therefore, this compartmentalisation has an impact on the flow of the hydrocarbons in the area, because the connectivity is low. This would ultimately impact the economic potential of extraction, consequently hydraulic fracturing would need to be implemented to increase the flow of the hydrocarbons. The tight reservoirs also relates to the reason for the low volume of recoverable gas in the two target areas. Despite the larger bulk volume of space available in these areas the fact that the permeability is low would result in the amount of gas recoverable to be generally poor.

This may not be economically viable as there is evidence of gas seepages in the Orange Basin. Multiple studies have been undertaken to understand the occurrence of gas seepages in the Orange Basin (Zvi Ben-Avraham *et al*., 2002, Loncke and Mascle, 2004, Paton *et al*., 2007). When gas seepages occur on the seafloor, it shows that there is vertical migration of gas. Evidence of gas seepages can be seen through the present of pock marks, carbonate mounds, giant gas chimneys and mud volcanoes on the sea floor (Loncke and Mascle, 2004). In the Orange basin, the gas seepage is a result of the presence of a hydrocarbon system below the sea floor (Zvi Ben-Avraham *et al*., 2002). Paton *et al*. (2007) proposed that there is the presence of hydrocarbon leakage in the southern region of the Orange Basin, which is caused by spatial and temporal changes in the post-rift overburden deposition.

For a reservoir to be considered as pay, it must have a porosity value of at least 10 %, volume of shale less than 40 % and water saturation of not more than 65 % (Opuwari, 2010). Referring to Table 6.3, the porosity value is 23 %, the volume of shale is 36 % and the water saturation is 65 %. The water saturation is very high and the volume of

shale, although it is within the net pay values, it is very close to falling outside of those parameters. In Table 6.4, the porosity value is 11 %, the volume of shale is 29 % and the water saturation is 64%. The lower shale volume is attributed to a large portion of Target Area 2, being comprised of basement. However, the porosity value is very low and the water saturation is high, similar to Target Area 1. Technically, these values fall within the net pay parameters. However, they are very close to falling outside of these parameters. Thus, both Target Area 1 and Target Area 2 aren't economically viable.

A study by Boyd *et al*. (2011) on a larger area of the Orange Basin was conducted. This study found that a large portion of the basin was scattered with gas chimneys that were either structurally controlled or stratigraphically controlled. These chimneys either end on the seafloor, or below the Miocene sequence as paleo-pock marks (Boyd *et al*., 2011). In addition to these chimneys, giant gas chimneys were also identified. However, according to Boyd *et al*. (2011), the presence of these giant gas chimneys are a result of paleo-gas escape structures. This is due to the fact that there is no activity of turbidity or pull downs within the gas structures, even though gas was identified in these structures. Lastly, Boyd *et al*. (2011) suggests that the gas migrates laterally up-dip from the Lower Aptian and the Barremian source rocks to the proximal areas of the basin. The gas then migrates further to just below the Cenomanian/Turonian sequence, which becomes a regional seal.

In addition to the sand, silt and shale facies identified in Target Area 2, a basement facies is present too. This facies marked and sits below the 6At1 sequence boundary. In the past, exploration in basement rock were never explored. However, due to the increase in demand for hydrocarbons and improved technology, exploration in alternative reservoir rock (such as basement rock) is beginning to expand. As mentioned in the well report for A-C3, the basement facies is made up of basaltic lavas interbedded with aphanitic tuffs. Although hydrocarbons are most commonly found in sedimentary rock, a few studies have shown that, hydrocarbons can occur in igneous rock (Gunterberg, 2013). The porosity and permeability can increase in areas where the basement rock has undergone weathering and fracturing (Gunterberg, 2013). Through this process, hydrocarbons can filter its way down into the basement rock

from surrounding sedimentary reservoirs. This could have possibly happened in Target Area 2.

In the southern region of the Siberian Platform, hydrocarbons were found to have infiltrated into the basement beneath the petroleum reservoir, where extraction was taking place. The characteristics they identified to be a promising reservoir were the identification of “black” zircons and multi-layered oil reservoirs, which are a result of deep occurring faults (Skvortsov, 2020).

7. CHAPTER 7: Conclusion

This study focussed on a small triangulated area in the southern part of the Orange Basin, however the seismic lines extend out of this area.

Target Area 1 and *Target Area 2* were the two areas of interest identified were bound between the M2KI and 13At1, and the TFLUVIAL and Bottom of Log in A-C3 respectively. Target Area 1 was present in all three wells and at a shallower depth than Target Area 2. Overall, Target Area 1 consisted of mostly silty shale and shaly silt. Although, there was a thin sand package at the top of the target area. Target Area 2, has considerably more sand and basement layers and thus the porosity and permeability are slightly better, but overall still poor.
Despite there being a bulk volume of space greater than 150 000 cubic metres in both areas, the recoverable gas is 151 923 cubic metres in Target Area 2. In Target Area 1, it is even less than that with a recoverable gas volume of 95 057 cubic metres. The water saturation is also lower than in Target Area 1. Comparing the two areas in terms of economic potential, Target Area 2 would be the area to look at, as it has slightly better economic properties than Target Area 1.

The analyses of the well reports A-C1, A-C2 and A-C3 signified that the three wells are dry. Thus, the study showed that the area is not economically viable though there is gas present. The permeability and porosity are poor, There is a high chance of water saturation in both target areas, but slightly more in Target Area 1. There is evidence of gas migration from hydrocarbon reservoirs either up to the surface or sitting in the just below the surface. Lastly, one of the potential reservoirs extend past the 6At1 sequence boundary, which is the basement. Basement exploration does occur, but it is not a common practice. Although there is gas present in the basement, it is unsure on how deep it goes. These wells were drilled to depths greater than 4km, thus in order to drill even deeper will be very costly.

In both January and February 2022, Shell and Total Energies respectively made two big petroleum finds in the Orange Basin (Bate, 2022). These two discoveries, concretely places the Orange Basin as one of the world's most exciting areas for

hydrocarbon exploration. There is still a massive demand for oil and gas, particularly gas, which more so is being recognised as a green source of energy. Revisiting previously studied areas, like in this study, are critical in finding resources that were once previously missed due to the lack of the modern technology and software. There is evidence of hydrocarbons, thus putting more research and development into this area can aid petroleum companies with their exploration.

A recommendation would be to continue to map the identified reservoirs along the seismic lines to identify how far they expand in the southern region of the Orange Basin. The geological reports were not examined in detail until the modelling was completed to avoid having a bias being created to the original well reports.

Another recommendation would be for future studies to collect more data. The seismic lines were 2-D seismic lines, although they were suitable for this study, 3-D or even 4-D seismic lines could be very effective. One of the main problems that occurred during this study was missing data particularly in the well logs. In A-C1, there was missing RHOB data from 3635 m – 4023 m. This depth coincided with a potential sandstone reservoir. Shallow sub-bottom data could provide critically information on exact locations of the presence of pockmarks and other gas seepage structures and if they are active or not.

8. References

AFRICA, R. H. 2016. *Reservoir Characterization using Genetic Inversion and Seismic attributes of Block 1 Orange Basin, Offshore South Africa.* Masters of Science, University of the Western Cape.

ARCHIE, G. E. 1942. The Electrical Resistivity Log as an Aid in Determining Some Reservoir Characteristics. *Transactions of the AIME,* 146**,** 54-62.

AUSTIN, J. A. & UCHUPI, E. 1982. Continental-oceanic crustal transition off southwest Africa. *AAPG Bulletin,* 66**,** 1328-1347.

BAHADORI, A. 2014. Overview of Natural Gas Resources. *Natural Gas Processing.* 1st ed.: Gulf Professional Publishing.

BAKER, R. O., YARRANTON, H. W. & JENSEN, J. L. 2015. 9 - Openhole Well Logs—Log Interpretation Basics. *Practical Reservoir Engineering and Characterization.*

BARTON, K. R., MUNTINGH, A. & NOBLE, R. D. P. 1993. Geophysical and Geological studies applied to hydrocarbon exploration on the West Coast Margin of South Africa. *Extended abstract of the third International Congress of the Brazilian Geophysical Society***,** 7-11.

BASHIR, Y., FAISAL, M. A., BISWAS, A., BABASAFARI, A. A., ALI, S. H., IMRAN, Q. S., SIDDIQUI, N. M. & EHSAN, M. 2021. Seismic expression of miocene carbonate platform and reservoir characterization through geophysical approach: application in central Luconia, offshore Malaysia. *Journal of Petroleum Exploration and Production,* 11**,** 1533–1544.

BATE, F. 2022. Shell and Total Namibia oil discoveries likely in billions of barrels - minister. *Reuters*.

BAUM, G. R. & VAIL, P. R. 1988. *Sequence stratigraphic concepts applied to Paleogene outcrops, Gulf Atlantic basins. In: sea level changes: an integrated approach.*, S.E.P.M Sp. Pub.

BIGELOW, E. L. 2002. *Introduction to Wireline Log Analysis,* Houston, Texas, Baker Atlas.

BOTT, M. H. P. 1980. Problems of passive margins from the viewpoint of the geodynamics project: a review. *Philosophical Transactions of the Royal Society of London,* 294**,** 5-16.

BOYD, D., ANKA, Z., DI PRIMO, R., KUHLMANN, G. & DE WIT, M. J. 2011. PASSIVE MARGIN EVOLUTION AND CONTROLS ON NATURAL GAS LEAKAGE IN THE ORANGE BASIN, SOUTH AFRICA *South African Journal of Geology,* 3-4**,** 415–432.

BROAD, D. S., JUNGSLAGER, E. H. A., MCLACHLAN, I. R. & ROUX, J. 2006. Offshore Mesozoic Basins. *In:* JOHNSON, M. R., ANHAEUSSER, C. R. & THOMAS, R. J. (eds.) *The Geology of South Africa.* Johannesburg: Geological Society of South Africa & Council for Geosciences.

BROWN, L. F., BENSON, J. M., BRINK, G. J., DOHERTY, S., JOLLANDS, A., JUNGSLAGER, E. H. A., KEENAN, J. H. G., MUNTINGH, A. & VAN WYK, N. J. S. 1995. Sequence stratigraphy in offshore South African divergent basins. An Atlas on Exploration for Cretaceous Lowstand traps.

BROWNFIELD, M. E. 2016. Assessment of Undiscovered Oil and Gas Resources of the Orange River Coastal Province, Southwest Africa. *In:* BROWNFIELD, M. E. (ed.) *Geologic Assessment of Undiscovered Hydrocarbon Resources of Sub-Saharan Africa.* U.S. Geological Survey Digital Data Series.

CAMPHER, C. 2009. *Geological modeling of the offshore Orange Basin, west coast of South Africa.* MSc, University of the Western Cape.

CATUNEANU, O. 2002. Sequence Stratigraphy of clastic systems: concepts, merits, and pitfalls. *Journal of African Earth Sciences,* 35**,** 1-43.

CATUNEANU, O. 2006. *Principles of Sequence Stratigraphy*, Elsevier.

CIVAN, F. 2007. CHAPTER 3 - PETROGRAPHICAL CHARACTERISTICS OF PETROLEUM-BEARING FORMATIONS. *Reservoir Formation Damage Fundamentals, Modeling, Assessment, and Mitigation.* 2nd ed.: Gulf Professional Publishing.

CUNHA, L. 2004. Integrating static and dynamic data for oil and gas reservoir modelling. *Journal of Canadian Petroleum Technology,* 43.

DE VERA, J., GRANADO, P. & MCCLAY, K. 2010. Structural evolution of the Orange Basin gravity-driven system, offshore Namibia. *Marine and Petroleum Geology,* 27**,** 223-237.

DE WET, W. M. 2012. *Bathymetry of the South African Continental Shelf.* Masters, University of Cape Town.

DINGLE, R. V., SIESSER, W. G. & NEWTON, A. R. 1983. *Mesozoic and Tertiary Geology of Southern Africa,* Rotterdam, A.A. Balkema.

DONALDSON, E. C. & TIAB, D. 2015. *Petrophysics*, Gulf Professional Publishing.

EGBELE, E., EZUKA, I. & ONYEKONWU, M. O. 2005. Net-To-Gross Ratios: Implications in Integrated Reservoir Management Studies. *29th Annual SPE International Technical Conference and Exhibition.* Abuja, Nigeria: Society of Petroleum Engineers.

EVANS, W. S. 1996. Technologies for multidisciplinary reservoir characterization. *Journal of Petroleum Technology*, 24-25.

FLORES, R. M. 2014. Chapter 7 - Coalbed Gas Production. *Coal and Coalbed Gas.* First Edition ed. Waltham, USA: Elsevier.

FRANK, J., COOK, M. & GRAHAM, M. 2008. *Developments in petroleum geoscience, Hydrocarbon Exploration and Production*.

GERRARD, T. & SMITH, G. C. 1982. Post-Paleozoic succession and structure of the southwestern African continental margin. *In:* WATKINS, J. S. & DRAKE, C. L. (eds.) *Studies in continental margin geology.* AAPG.

GUNTERBERG, L. 2013. *Oil occurrences in crystalline basement rocks, southern Norway – comparison with deeply weathered basement rocks in southern Sweden* Lund University.

HERBIN, J. P., MULLER, C., GRACIANSKY, P. C., DE JACQUIN, T., MAGNIEZ-JANNIN, F. & UNTERNEHR, P. 1987. Cretaceous anoxic event in the South Atlantic. *Revista Brasileria de Geociencia,* 17, 92-99.

JOLLEY, S. J., FISHER, Q. J. & AINSWORTH, R. B. 2010. Reservoir Compartmentalization: An Introduction. *Geological Society London Special Publication,* 347, 1-8.

JUNGSLAGER, E. H. A. 1999. Petroleum habitats of the Atlantic margin of South Africa. *The oil and gas habitats of the South Atlantic.* London: Geological Society.

KAMGANG, T. 2013. *Petrophysical evaluation of four wells within Cretaceous gas-bearing sandstone reservoirs in blocks 4 and 5 Orange Basin, South Africa.* Master of Science, University of the Western Cape.

LARSEN, M. 1994. Geological well completion report of borehole A-C3. SOEKOR (Pty) Ltd.

LONCKE, L. & MASCLE, J. 2004. Mud volcanoes, gas chimneys, pockmarks and mounds in the Nile deep-sea fan (Eastern Mediterranean): Geophysical evidences. *Marine and Petroleum Geology,* 21, 669-689.

MA, Z. Y. 2011. Reservoir Characterization: A look back and ways forward. *AAPG Bulletin*.

MABONA, N. I. 2012. *Application of petrophysics and seismic in reservoir characterization. A case study on selected wells, in the Orange Basin, South Africa.* Master of Science, University of the Western Cape.

MAGOON, L. B. & DOW, W. G. 1994. The petroleum system. *In:* MAGOON, L. B. & DOW, W. G. (eds.) *The Petroleum System: From Source to Trap.* American Association of Petroleum Geologists.

MITCHUM JR, R. M. 1977. Seismic Stratigraphy and Global Changes of Sea Level: Part 11. *Application of Seismic Reflection Configuration to Stratigraphic Interpretation.*

MORRIS, R. L. & BIGGS, W. P. 1967. Using log derived values of water saturation and Porosity. *SPWLA 8th Annual Logging Symposium.* Denver, Colorado.

MUGIVHI, M. H. 2017. *Integration of petrographic and petrophysical logs analyses to characterise and assess reservoir quality of the Lower Cretaceous sediments in the Orange Basin, offshore South Africa.* Master of Science, University of the Western Cape.

MUNTINGH, A. & BROWN, L. F. 1993. Sequence Stratigraphy of Petroleum Plays, Post – Rift Cretaceous Rocks (Lower Aptian to Upper Maastrichtian), Orange Basin, Western Offshore, South Africa. AAPG.

MUTINGH, A. 1993. Geology, prospect in Orange Basin offshore western South Africa. *Oil Gas Journal***,** 106-109.

NORTH, F. K. 1985. *Petroleum Geology*, Springer.

NUMMEDAL, D. & SWIFT, D. J. P. 1987. Transgressive stratigraphy at sequence bounding unconformities: some principles derived from Holocene and Cretaceous examples. *In:* NUMMEDAL, D., PILKEY, O. H. & J.D., H. (eds.) *Sea level fluctuations and coastal evolution.* Econ. Paleontol. Mineral. Spec. Pub.

NUSSBAUMER, R., MARIETHOZ, G., GLOAGUEN, E. & HOLLIGER, K. 2017. Which Path to Choose in Sequential Gaussian Simulation. *Mathematical Geosciences,* 50**,** 97–120.

OPUWARI, M. 2010. *Petrophysical evaluation of the Albian age gas bearing sandstone reservoir of the O-M field, Orange Basin, South Africa.* Ph. D. thesis, University of the Western Cape.

PASA 2019. Petroleum Exploration Information and Opportunities brochure. Petroleum Agency of South Africa.

PATON, D. A., PRIMO DI, R., KUHLMANN, G. & HORSFIELD, B. 2007. Insights into the Petroleum System Evolution of the southern Orange Basin, South Africa. *South African Journal of Geology,* 110**,** 261–274.

POSAMENTIER, H. W. & ALLEN, G. P. 1999. Siliciclastic Sequence Stratigraphy: concepts and applications. *SEPM Concepts in Sedimentology and Paleontology.*

RIDER, M. H. 1996. *The geological interpretation of well logs*, Rider – French consulting limited.

SCHLUMBERGER 2004. Petrel Velocity Modelling Training and Exercise guide. 14 ed.

SERRA, O. & SULPICE, L. 1975. Sedimentological analysis of sand shale series from well logs. *SPWLA 16th Ann. Symp. Trans., paper W.***,** 1-23.

SHAHBAZI, A., MONFARED, M. S. & ANATOLIEVICH, S. V. 2019. Integrated strategy for porosity mapping using genetic inversion on heterogeneous reservoir. *ASEG Extended Abstracts,* 2019**,** 1-4.

SKVORTSOV, V. A. 2020. Assessment of the Oil and Gas Potential of the Basement of the Southern Part of the Siberian Platform and Deep-Seated Oil Exploration. *Doklady Earth Sciences,* 492**,** 302–305.

SOEKOR 1991. A-C1 Geological Well Completion Report. SOEKOR (Pty) Ltd.

SPWLA 1975. Glossary of terms & expressions used in well logging. *150 technical questions and answers for job interview Offshore Oil & Gas Platforms.* Houston, Texas: Society of Professional Well Log Analysts.

STEIBER, S. J. 1970. Pulsed Neutron Capture Log Evaluation. *Fall Meeting of the Society of Petroleum Engineers of AIME.* Houston, Texas.

TIMUR, A. 1968. An Investigation of Permeability, Porosity and Residual Water Saturation Relationships for Sandstone Reservoirs. *The Log Analyst,* 9**,** 8-17.

TURNER, S., KELLEY, S., HAWKESWORTH, C. J. & MANTOVANI, M. 1994. Magmatism and continental break-up in the South Atlantic: high precision 40Ar-39 geochronology. *Earth and Planetary Science Letters,* 121**,** 333-348.

VAN DER SPUY, D. 2003. Aptian source rocks in some South African Cretaceous basins. *In:* ARTHUR, T. J., MACGREGOR, D. S. & CAMERON, N. R. (eds.)

Petroleum Geology of Africa: New Themes and Developing Technologies. London: The Geological Society of London.

VAN WAGONER, J. C., POSAMENTIER, H. W., MITCHUM, R. M., VAIL, P. R., SARG, J. F., LOUTIT, T. S. & HARDENBOL, J. 1988. An overview of sequence stratigraphy and key definitions. *In:* WILGUS, C. K., HASTINGS, B. S., KENDALL, C. G. S. C., POSAMENTIER, H. W., ROSS, C. A. & VAN WAGONER, J. C. (eds.) *Sea Level Changes—An Integrated Approach.* SEPM Special Publication.

WATKEYS, M. K. 2006. Gondwana Break-Up: A South African Perspective. *In:* JOHNSON, M. R., ANHAEUSSER, C. R. & THOMAS, R. J. (eds.) *The Geology of South Africa. Geological Society of South Africa.* Pretoria: Geological Society of South Africa.

WILLIAMS, A. 2018. *Reservoir Characterization of well A-F1, Block 1, Orange Basin, South Africa.* Master of Science, University of the Western Cape.

YELWA, N. A., MUSTAPHA, K. A., OPUWARI, M. & HAKIMI, M. H. 2022. Shale-gas potential from Cretaceous succession in South Africa's Orange Basin: Insights from integrated geochemical evaluations. *Marine Georesources & Geotechnology*.

ZVI BEN-AVRAHAM, Z., SMITH, G., RESHEF, M. & UNGSLAGER, E. 2002. Gas hydrate and mud volcanoes on the southwest African continental margin off South Africa. *Geology,* 30**,** 927–930.